引用格式：YI Li, HAN Haobin, LI Zhekai, et al. Near-infrared Single-photon Lidar for Gas Remote Sensing: Technologies and Applications (Invited)[J]. Acta Photonica Sinica, 2026, 55(5):0555210
易丽,韩豪彬,栗喆锴,等.近红外单光子气体遥感激光雷达及应用(特邀)[J].光子学报,2026,55(5):0555210

近红外单光子气体遥感激光雷达及应用(特邀)

易丽[1,2],韩豪彬[1,2,3],栗喆锴[1,2,3],许可祎[1,2],胡佳栋[1,2,3],余赛芬[1,2],
章振[1,2,3],夏海云[1,2,3]

(1 南京信息工程大学 大气物理学院,南京 210044)
(2 气候系统预测与变化应对全国重点实验室,南京 210044)
(3 杭州光在科技有限公司,杭州 310005)

摘 要:近红外光因其气体吸收线覆盖丰富、太阳光辐射相对紫外和可见光较弱、光电器件成熟等因素,成为了气体遥感的重点研究和应用的光学波段。单光子探测技术不仅具有极灵敏的激光大气后向散射信号探测能力,还为近红外气体遥感系统在多气体探测、系统小型化和稳定性方面提供了新的发展方向。首先,对当前近红外单光子探测技术进行了总结和比较。其次,聚焦单光子探测技术在气体遥感领域的研究现状展开系统性综述,根据探测原理和性能对当前的实用型技术进行了分类。重点关注基于近红外单光子探测技术的差分吸收激光雷达、路径积分吸收激光雷达和差分吸收光谱激光雷达在不同场景下的气体遥感表现。最后,对近红外单光子技术在气体遥感上的应用进行了总结和展望。

关键词:单光子探测;近红外气体遥感;差分吸收;路径积分;光谱遥感
中图分类号:P407 **文献标识码**:A **doi**:10.3788/gzxb20265505.0555210

0 引言

气体光学遥感作为环境监测、工业安全及气候变化研究的关键技术手段,近年来在全球范围内获得了广泛关注与快速发展。随着“双碳”战略的深入推进,工业安全、环境监测等领域对痕量气体、易燃易爆及有毒有害气体的探测要求不断提高。除了对高性能激光光源的需求外,探测器的性能是影响激光雷达系统性能的另一重要因素[1]。传统激光雷达采用的模拟探测器在工作机制上受限于光电转换过程中的散粒噪声及后端读出电路的热噪声,需要在光较强的大气回波信号条件下形成光电流,经过光电转换和模数转换后进行探测[2]。因此,提高激光雷达探测能力的传统方法,通常依赖提高激光器的功率或者望远镜的面积。然而,这类方法在能耗、系统体积及工程实现等方面受到一定限制。

在此背景下,单光子探测器(Single-Photon Detector, SPD)因其具有高灵敏度、低噪声、数字化的特征,为激光雷达的发展提供新的方向[3]。相干探测激光雷达的灵敏度理论上也可以达到量子极限,并且响应带宽一般在0.1~1 GHz(超窄带宽的背景光抑制能力),在大气风场测量等领域已获得广泛应用[4-9]。相干探测本质上是单模、单偏振态外差探测。在激光雷达遥感中,大气后向散射信号受大气湍流引发的波前畸变(退相干)、焦面光斑弥散抖动(耦合效率降低)及气溶胶米散射退偏振等多重因素影响,使得这种机制在远距离、高精度气体遥感应用中面临挑战。

本文围绕近红外SPD技术在气体遥感领域的应用现状展开综述。首先介绍SPD技术的分类和应用;随后按照气体遥感探测机制,对基于近红外SPD技术的激光雷达进行分类和对比;最后对未来该领域的研究方向进行了展望。

基金项目:国家自然科学基金(42405138,42305147)
第一作者:易丽,202512030326@nuist.edu.cn
通讯作者:夏海云,hsia@ustc.edu.cn
收稿日期:2026-04-06;**录用日期**:2026-05-10

1 近红外SPD技术分类和比较

SPD是一类能够对极微弱信号(单光子或者数个光子)进行高灵敏探测的设备。常见的SPD类型包括光电倍增管(Photomultiplier Tube, PMT)、单光子雪崩二极管(Single-Photon Avalanche Diode, SPAD)、超导纳米线单光子探测器(Superconducting Nanowire Single-Photon Detector, SNSPD)以及频率上转换单光子探测器(Upconversion Single Photon Detector, UCSPD)等。PMT基于材料的外光电效应,将入射光子转换为光电子,并通过多级倍增实现高增益输出,具有响应速度快、技术成熟等优点,但体积较大且需要高压供电。PMT在紫外-可见光波段探测甲烷(Methane, CH_4)、二氧化碳(Carbon Dioxide, CO_2)、臭氧(Ozone, O_3)、水汽(Water Vapor, H_2O)、气溶胶等方面均有应用[10]。SPAD依托半导体PN结的雪崩倍增效应,在室温或普通制冷条件下实现单光子探测。该类器件体积小、易集成,但暗计数率和后脉冲效应的影响不可忽略。相关应用涵盖大气折射率结构常数反演及痕量气体探测等[11]。SNSPD利用超导纳米线在低温下的超导相变实现单光子探测,具有高探测效率、无后脉冲效应及优异的时间分辨率等优势,已被应用于近红外波段气体探测(如CO_2、CH_4、氨气(Ammonia, NH_3))、风速[12]以及气溶胶探测等[13-14]。UCSPD则通过非线性光学过程将近红外光子上转换为可见光,再由可见光探测器进行光电转化,从而实现近红外探测的高灵敏度与低噪声。该技术已经应用于大气能见度反演[15]、风速[16]探测等领域。

20世纪30年代PMT出现后,其在紫外-可见光波段气体遥感领域的应用逐渐突出,被广泛用于O_3[17-26]、H_2O[27-39],二氧化硫(Sulfur Dioxide, SO_2)[40-41]等气体的遥感探测。尽管PMT在近红外波段响应度远低于紫外和可见光波段,但在弱信号探测能力上仍优于传统光电探测器,因此早期PMT也被应用于近红外波段进行温室气体的遥感探测。近红外波段是多种气体分子识别与定量分析的“指纹波段”[42],并且该波段大气透过率高,受太阳光背景干扰相较于可见光波段更小,更适配全天时遥感的需求。随着InGaAs/InP、Si-SPAD技术的发展与成熟,SPD在近红外波段的探测效率提升[43]。近年来UCSPD技术以及SNSPD技术的发展,更是增强了该波段单光子探测能力[44-45]。

目前近红外波段主要采用的探测器包括SPAD、UCSPD以及SNSPD,表1总结了应用在气体探测领域的这三类探测器的关键性能指标。其中,SNSPD具有最高探测效率和最低暗计数,无死时间与皮秒级时间抖动,但需要液氦制冷保证工作温度在3 K以下。UCSPD通过频率上转换将单光子频率近红外波段转到可见光波段,利用Si-SPAD或者PMT进行探测。该器件可以在室温下工作,但是泵浦光的频率稳定性和周期极化铌酸锂波导的温度漂移会对上转换效率产生影响。以上两类探测器一般采用单模探测方式,通过并行设计,也能实现多通道(多模)探测。InGaAs/InP SPAD相对于其他两类探测器,探测效率较低,暗计数水平较高,存在纳秒至微秒量级的死时间(为了抑制后脉冲现象)。但其系统结构最简单,通过校准,仍可以实现精密探测,因此应用最为广泛。

表1 典型SPD性能参数

Table1 Performance parameters of typical SPD

SPD type	Detection efficiency	Dark count	Dead time	Time jitter	Maximum count rate	Working temperature	Afterpulse probability	References
InGaAs/InP	10%@1 550 nm	950 cps	600 ns	200 ps	1.6 MHz	223 K	18%	[47][48]
UCSPD	20%@1 548 nm	300 cps	50 ns	350 ps	15 MHz	300 K	0.3%	[15][49]
SNSPD	32%@1 572 nm	100 cps	0	~50 ps	20 MHz	2.3 K	0	[50]
	93%@1 550 nm	1 cps	0	~150 ps	25 MHz	120 mK	0	[51]

除上述光电性能指标外,还需考虑探测器的光敏面尺寸。因大气湍流会导致焦平面光斑的弥散和抖动,采用大光敏面探测器可以提高空间光到光纤或者后继光路的耦合效率。SNSPD为实现大面元探测需采用多路并行结构[46],目前光敏面尺寸达到200 μm。因需要多通道同时工作,定制良品率低,成本高。InGaAs/InP SPAD的光敏面尺寸范围通常在9 μm至100 μm之间,但随着光敏面尺寸增大,暗计数增加;UCSPD受限于上转换波导器件的尺寸,并考虑泵浦光功率的需求,通常用于9 μm的单模光敏面转换。

2 近红外单光子气体遥感激光雷达分类

气体遥感技术是一种高效、大范围的监测手段，已成为国内外科研领域的研究热点。欧美发达国家较早布局气体遥感技术，美国国家航空航天局（NASA）、欧洲空间局（ESA）、美国国家标准与技术研究院（NIST）等机构先后发展了多套星载、机载及地基激光雷达系统，用于温室气体与大气污染物的监测，例如ASCENDS[52-55]（Active Sensing of CO_2 Emissions over Nights, Days, and Seasons）、MERLIN[56-57]（Methane Remote Sensing Lidar Mission）、CHARM-F[58-59]（CO_2 and CH_4 Remote Monitoring—Flugzeug）等任务。国内科研院所与高等院校，在气体遥感领域的研究也做出世界前沿的工作[60]。中国科学院上海光学精密机械研究所陈卫标团队[61-63]成功研制国际首台CO_2和气溶胶联合探测激光雷达，于2022年搭载在“大气”一号卫星（DQ 1）发射升空，实现了全球温室气体高精度激光遥感。大连理工大学梅亮团队[64-66]采用沙氏成像激光雷达对气体进行遥感，取得了系列创新性成果。武汉大学龚威团队[67-70]发展了机载红外差分吸收激光雷达及基于高光谱卫星的CH_4排放反演技术，致力于大气成分遥感、激光雷达系统设计与性能提升，并牵头成立了碳中和感知与效能评估教育部工程研究中心。浙江大学刘东团队[71-74]聚焦环境激光雷达（大气、海洋及星载等）光电检测与遥感领域的前沿研究，在污染气体及温室气体遥感探测方面取得了一系列创新性成果。中国科学院安徽光学精密研究所团队[75-78]在紫外到可见光波段，开展大气O_3、CO_2、二氧化氮（Nitrogen dioxide, NO_2）等气体的理论和实验研究。中国科学技术大学刘诚团队[79-82]专注天空地一体化超光谱遥感与人工智能技术研究，自主研发了国产紫外可见超光谱卫星遥感反演技术，实现国产卫星遥感的突破。南京信息工程大学夏海云团队[50,83-86]和卜令兵团队[87-89]长期致力于温室气体遥感和研究，在高光谱分辨率激光雷达、星载探测机载验证及数据分析方面取得了重要进展；北京理工大学研究团队[90-92]在非制冷红外成像、激光雷达等气体遥感领域，实现了对多种工业危险气体、温室气体的远距离成像检测与定位。鉴于该领域的技术发展迅速，本文不能逐一列举相关工作。

在全球气体遥感技术快速发展和探测系统持续迭代的情形下，合理选择探测波段并推动探测技术创新，是进一步提升气体遥感精度的关键。近红外波段凭借大气穿透能力优异、太阳背景辐射干扰小等优势，成为气体遥感激光雷达探测的优选波段。但近红外光子能量较低，传统探测器在该波段的灵敏度受限，在进一步提升激光雷达性能上具有挑战性。基于单光子探测技术的近红外波段激光雷达，可以实现弱信号探测和累积，从而提升气体遥感的时空分辨率与探测精度。

在近红外波段，根据反演原理，将基于单光子探测技术实现大气气体探测的方法分为三类：具有距离分辨的差分吸收激光雷达（Differential Absorption Lidar, DIAL）、无距离分辨但可具有光谱分辨的路径积分吸收激光雷达（Integrated Path Absorption Lidar, IPAL）（根据具体实现手段，该方法细分为三种技术：路径积分差分吸收（Integrated Path Differential Absorption, IPDA）技术、路径积分双光梳光谱（Integrated Path Dual-Comb Spectroscopy, IPDCS）技术及路径积分扫描吸收光谱（Integrated Path Scanning Absorption Spectroscopy, IPSAS）技术）和既具有距离分辨又具有光谱分辨的差分吸收光谱激光雷达（Differential Absorption Spectroscopy Lidar, DASL）。根据探测场景的不同以及对性能指标需求的差异，结合各种技术的发展历程对以上激光雷达进行了回顾和分类。

2.1 差分吸收激光雷达

DIAL是一种基于差分吸收原理的主动光学遥感技术。其原理是在目标气体吸收线附近发射两束或多束不同波长的激光，并接收大气后向散射回波，利用不同波长在传播路径中所经历的吸收差异来反演目标气体浓度。其中在线波长（On-line）选取在目标气体吸收较强的位置，离线波长（Off-line）选取在吸收较弱或无吸收的位置，且两个波长间隔小，通常可认为除目标气体造成的吸收外，两波长在大气中其他的消光系数基本一致。通过比较两路回波信号随距离的强度差异，并结合目标气体吸收截面及系统参数，即可获得目标气体的浓度廓线[93-94]。由于DIAL的原始信号来自微弱的气溶胶的后向米散射，需通过长时间信号积累，提高系统探测信噪比。然而，这种长时间积累的信号处理方式会降低系统时间分辨率，难以快速响应大气气体浓度的瞬时动态变化，特别是在星载或机载等快速移动平台上。因此，DIAL通常应用于地基平台，对固定范围进行长时间连续观测，获取具有高距离分辨率的气体浓度空间分布。

基于DIAL，结合SPD搭建的系统主要应用于温室气体探测，例如CO_2、CH_4、H_2O。在近红外波段，

DIAL的探测性能受到多方面因素的影响。在设计激光雷达系统过程中，需要综合考虑目标气体吸收线的温度敏感性、压力展宽效应及其他干扰气体的影响。在实验过程中，激光器的频率稳定性与探测器自身的稳定性都会影响反演结果的精准度，系统中通常需要采用稳频、温控等措施提升系统自身的稳定性。此外，大气湍流会进一步导致激光在传播路径上随机扰动，引发回波信号的强度抖动。针对上述影响因素，需要在实验中进行校正与实施补偿，确保温室气体高精度探测[50]。

2009年，日本东京都立大学SAKAIZAWA D率先开发1.6 μm波段CO_2探测DIAL系统，利用准相位匹配光学参量振荡器（Optical Parametric Oscillator，OPO）实现高能量单频脉冲输出，并采用短波红外光子计数探测器PMT（H10330-75，Hamamatsu）构建系统[95]。选择对水汽干扰小且温度敏感度低的波长，在5.2 km以下实现了CO_2密度剖面统计误差小于2%。

2015年，美国国家大气研究中心SPULER S M团队研发出一款基于828 nm的SPD（SPCM-AQRH-13、SPCM-AQRH-13-FC，Excelitas）探测DIAL系统，实现了H_2O廓线遥感[96]。如图1所示，该系统采用高量子效率单光子探测器，因此可使用低能量二极管激光器。在野外实验中实现150 m分辨率的H_2O探测，0.3～4 km范围均值误差小于10%。该系统具备复杂干扰条件下（白天强光、多云等）的长期连续自主运行能力，为地基H_2O遥感网络建设奠定了技术基础。从以上两个工作来看，采用单光子技术DIAL可以降低激光出射功率的要求。

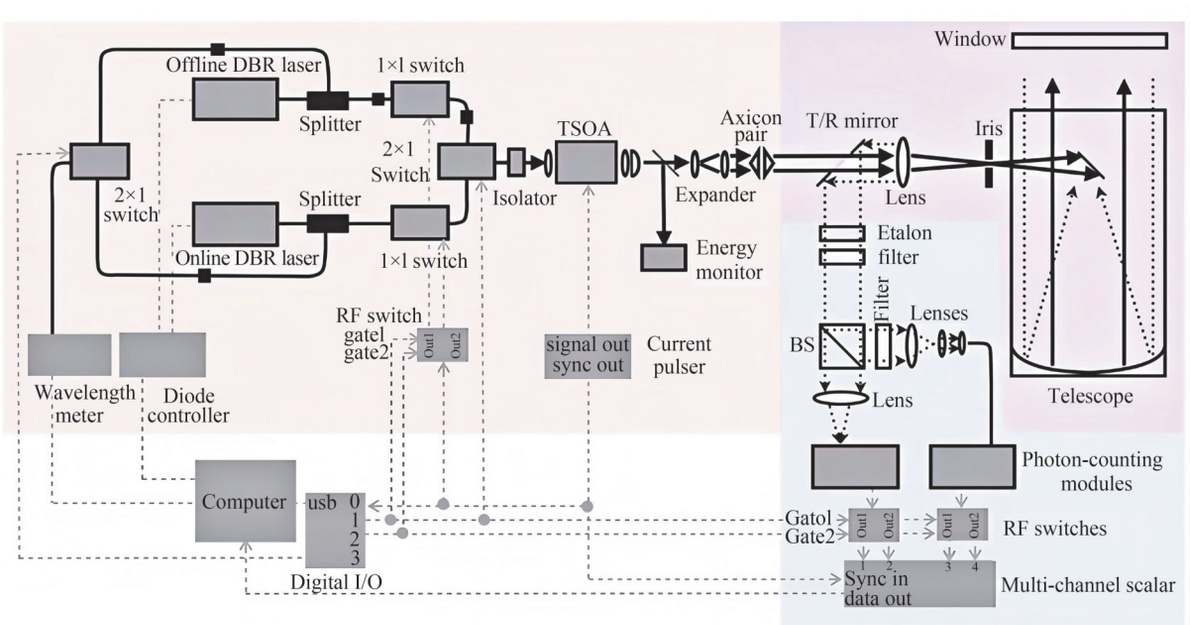

图1 H_2O DIAL系统原理图[96]

Fig.1 Schematic of the H_2O DIAL system[96]

2018年，美国NIST的WAGNER G A等建设1.6 μm波段DIAL系统，利用远近双探测通道，实现了CO_2和H_2O双气体距离分辨浓度同步探测[97]。在250 m距离分辨率、10 min时间分辨率下，在1 km探测距离实现了6 μmol/mol的CO_2和0.44 g/kg的H_2O干空气混合比探测精度。

同年，丹麦技术大学MENG L团队提出基于UCSPD技术的红外波段CH_4 DIAL系统，系统如图2所示。该团队研发了紧凑型UCSPD，通过PPLN晶体将CH_4在1 646 nm特征吸收波长的红外信号上转换至646 nm可见光波段，再由PMT（H7422-40，Hamamatsu）探测[98]。该团队工作实现45%的内部上转换量子效率，噪声等效功率显著优于传统InGaAs/InP APD。该系统成功实现3～9 km距离分辨的大气CH_4探测，图3展示了传统APD与UCSPD的探测对比结果，通过采用UCSPD实现了远距离信号信噪比以及差分吸收光学深度（Differential Absorption Optical Depth，DAOD）探测精度的大幅提高。

在研究碳源碳汇的过程中，相对于单一浓度测量，通量能直接反映出区域尺度上的气体净交换与输送过程，是定量评估碳源碳汇的关键参数[99]。2022年，岳斌等采用SNSPD实现了1 572 nm波段CO_2探测，同

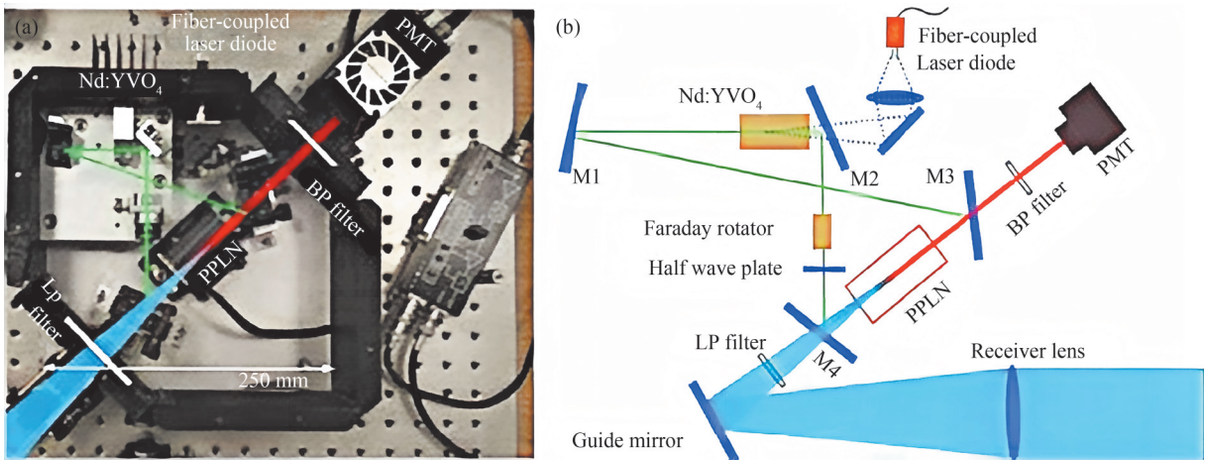

图2　UCSPD单光子探测系统。(a) UCSPD实物照片；(b) UCSPD光路结构示意图[98]

Fig.2　UCSPD single-photon detection system. (a) Photograph of the UCSPD instrument; (b) Schematic diagram of the optical path structure of the UCSPD[98]

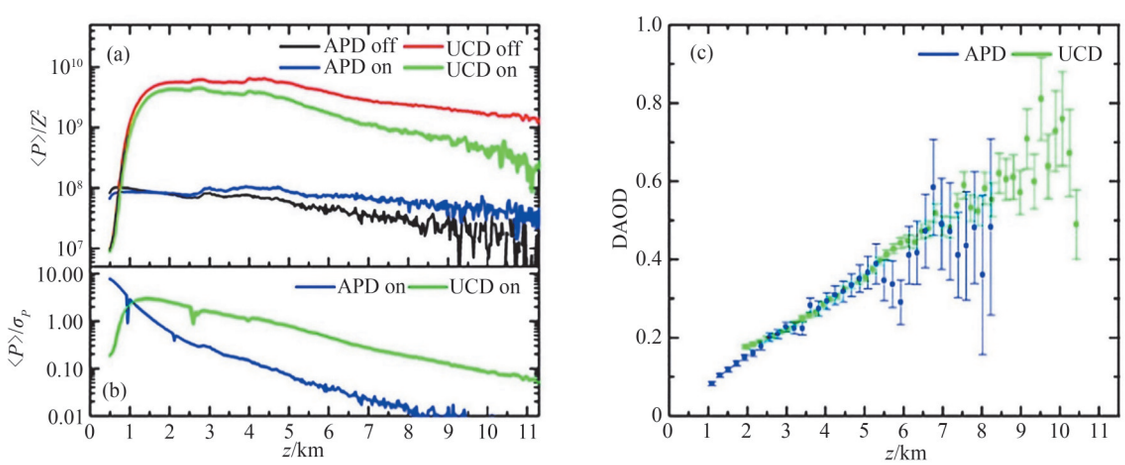

图3　APD与UCSPD探测结果对比图。(a) on和off距离校正后向散射信号随距离z的演化曲线；(b)信号平均幅值$\langle P\rangle$与其标准差σ_p之比（信噪比）随距离的变化曲线；(c)不同距离z处测得的DAOD对比结果[98]

Fig.3　Comparison detection results of APD and UCSPD systems. (a) Evolution curves of the backscattered signal versus distance z after on and off distance calibration; (b) Curves of the signal-to-noise ratio (the ratio of the average signal amplitude $\langle P\rangle$ to its standard deviation σ_p) versus distance; (c) Comparison results of the DAOD measured at different distances z[98]

时结合相干多普勒测风激光雷达，实现CO_2通量遥感，如图4所示[46]，并通过对接收光路中多模光纤的模式扰动与温度敏感性进行优化控制，提升了系统的稳定性。采用闭合边界积分法对局地CO_2净水平通量进行精准估算，能够有效监测CO_2局地排放。

为了提高DIAL的探测精度，2023年，美国NIST的STROUD J R基于PMT（H10330A-75 SEL、H12397-75，Hamamatsu）和OPO大能量激光器（5 mJ）搭建了多波长DIAL系统，如图5所示[100]。实现了10波长时分复用探测，成功应用于复杂光谱气体探测。实验显示，对构建的路径积分吸收激光雷达和距离平均的DIAL进行了验证对比，CO_2和CH_4的偏差在1%～2%量级。在此工作中，波长扫描的累计时间为10 min。在此期间，激光功率、路径中的大气湍流和气溶胶等因素均可能发生变化，从而导致远程回波信号强度和大气透过率的波动。因此本工作很难得到有距离分辨率的光谱，针对这一问题，本文将在2.2.3节中进一步讨论。

2025年，厦门大学上官明佳团队研发了基于SNSPD的CO_2 DIAL，实现了5 min时间积累下，8 km探测距离、30 m距离分辨率下的CO_2浓度探测，与原位观测数据标准差仅10 ppm（1 ppm=1×10^{-6}）[101]。同年，齐

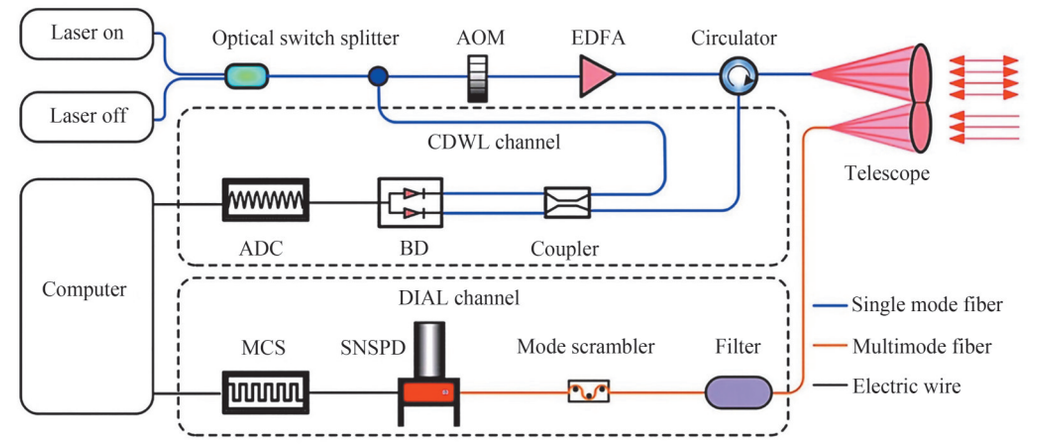

图4 CO_2混合激光雷达系统原理图[46]

Fig.4 Schematic diagram of the CO_2 hybrid lidar system[46]

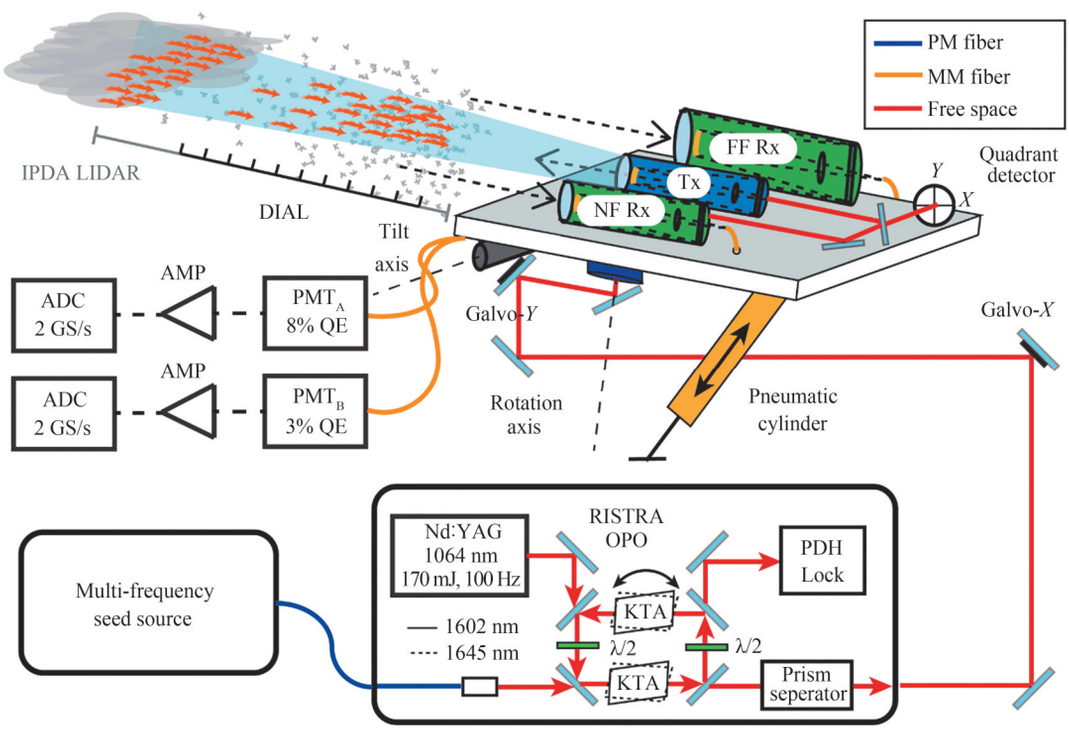

图5 CO_2、CH_4和H_2O DIAL/IPDA激光雷达光路图[100]

Fig.5 The optical system of the CO_2、CH_4 and H_2O DIAL/IPDA lidar[100]

鲁工业大学王章军团队搭建了基于1.5 μm双波长光纤激光器和InGaAs/InP的紧凑型DIAL[102]。实现了距离分辨率为25 m,时间分辨率为15 min的CO_2浓度探测。

2.2 路径积分吸收激光雷达

与DIAL依赖大气后向散射回波获取距离分辨浓度廓线不同,IPAL通常以地表、建筑物或云顶、角反射器等目标反射回波,再反演得到目标气体的路径积分浓度。IPAL按具体实现形式可分为三类技术:一类是基于双波长和多波长的IPDA技术;第二类是基于IPDCS技术;第三类是基于IPSAS技术。

2.2.1 路径积分差分吸收技术

IPDA接收来自硬目标或云层的后向散射信号,该信号强度远大于大气气溶胶后向散射回波信号,信噪比更强,因此适合快速远距离柱浓度探测。因为IPDA测量激光传输路径上气体柱浓度,吸收深度高,保证了探测灵敏度。相比于DIAL,IPDA具有高时间分辨率和浓度准确的特点。因此,IPDA通常被应用在星

载、机载等高速运动平台开展自顶向下的大尺度气体柱浓度遥感探测[103-105]。其中多频IPDA技术通过多频点采样和非线性拟合，进一步提高柱浓度反演精度，并增强了系统对复杂背景的适应能力和多气体场景的探测能力。

传统脉冲式IPDA激光雷达通常采用在线与离线波长顺序发射的工作方式，这种体制一方面依赖高能脉冲激光器，存在系统体积大、功耗高、效率偏低等问题；另一方面，由于两波长回波并非同时获取，易受到平台运动、指向漂移及地表反射不均匀性的影响，产生在线/离线光束的足迹失配，从而给柱浓度反演带来误差。针对上述问题，英国布里斯托大学AI X等在2016年提出了基于伪随机调制连续波和单光子技术探测的星载IPDA方案，通过在线与离线信号同步发射和相关解调实现差分吸收测量[106]。数值模拟结果表明，在2.5 W平均功率、50 km路径积分条件下，该方案理论上可实现约1.5 ppm的CO_2浓度反演精度。若采用100 pm超窄带滤波，可进一步将浓度精度提高至0.5 ppm。

基于上述模拟分析，德国航空航天中心QUATREVALET M等于2017年设计并搭建了一套基于随机调制连续波、混合MOPA发射机和单光子计数接收的IPDA激光雷达系统，如图6所示[107]。团队开展了约2 km水平路径CO_2测量，并通过与脉冲式CHARM-F系统及原位仪器对比，在7 s积分时间下实现了约0.63%～0.67%的DAOD随机误差，对应约2.5 ppm的CO_2浓度精度。同时，长期实验中系统相对原位测量表现出约±10%（约±40 ppm）的准确度。

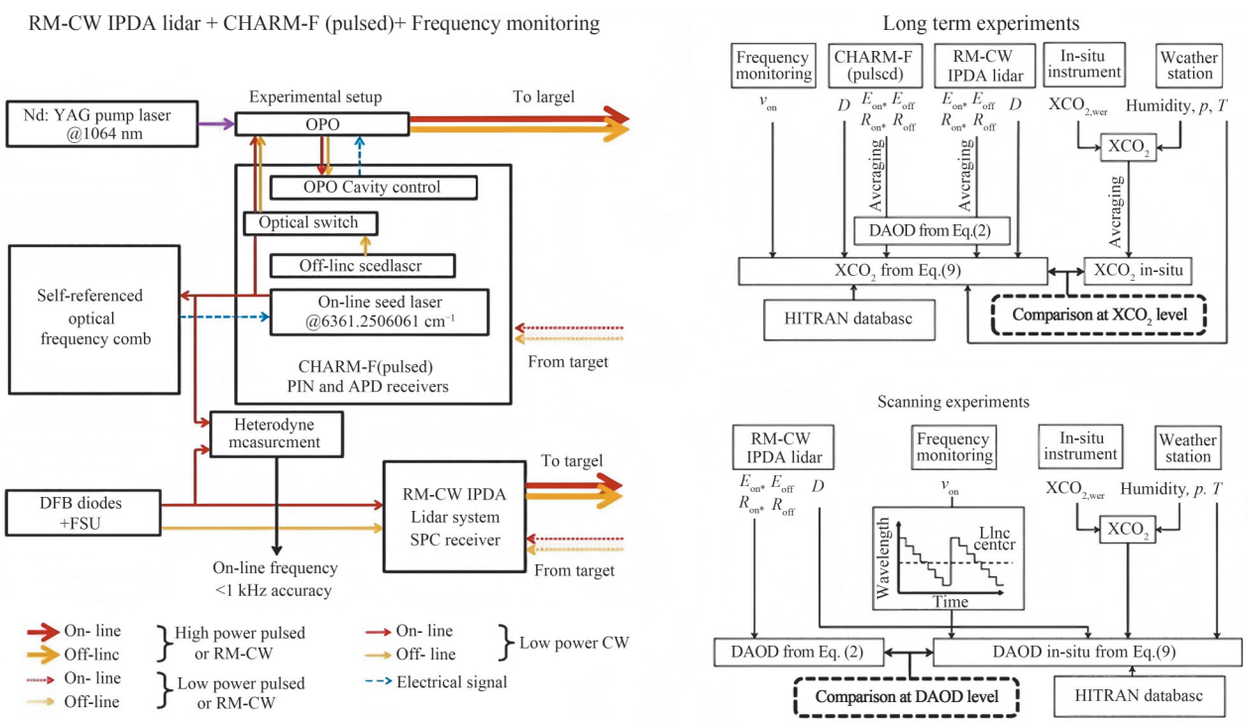

图6　RM-CW IPDA激光雷达原理图及长期实验与扫描实验的流程图[107]

Fig.6　Schematic diagram of RM-CW IPDA lidar and flowcharts for long-term experiment and scanning experiment[107]

2.2.2　路径积分双光梳光谱技术

不同于DIAL和IPDA主要依赖On-line和Off-line的差分吸收信号进行浓度反演，传统双光梳光谱技术是一种基于两列具有高相干性的光频梳进行外差拍频的探测方法。相比差分吸收方法，双光梳技术在光谱覆盖范围、频率精度及多组分同时探测方面具有明显优势[108-114]。近年来，结合SPD对弱信号的高灵敏探测能力，双光梳直接探测技术被用于开放环境中的气体遥感探测。

2025年，中国科学技术大学的薛向辉团队提出了单光子双光梳光谱方法，并构建了紧凑型全光纤系统，如图7所示[115]。在距离光源1.65 km的位置上放置了一个反射镜。采用两台InGaAs/InP SPD（QCD600B-H，Quantum-CTek）分别采集1 571 nm和1 573 nm波段微弱信号探测。该系统实现了在15 min时间分辨率和1.6 km开放路径对大气环境中CO_2、H_2O和HDO的连续遥感观测。

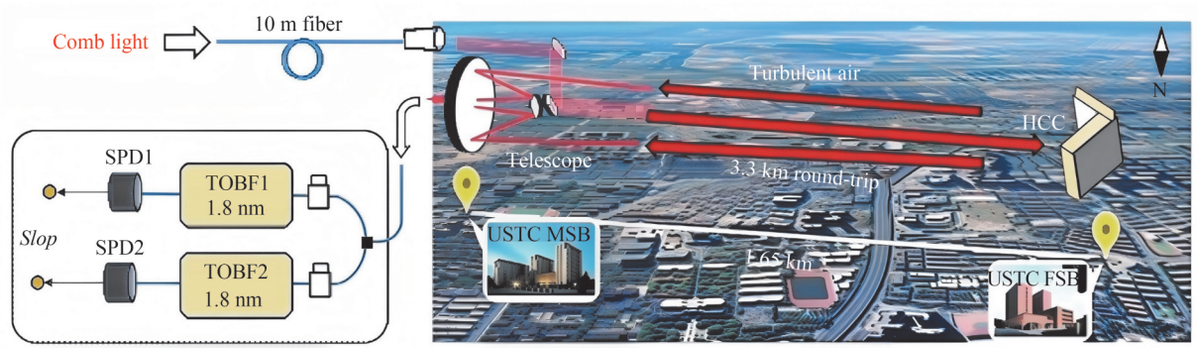

图7 开放式光子计数双光梳系统图[115]

Fig.7 Open-path photon-counting dual-comb system[115]

尽管双光梳技术具有宽光谱覆盖和高分辨率优势，但其总输出功率被分配到大量离散梳齿上，导致单个梳齿对应的有效信号功率较低。因此，传统双光梳遥感通常需要依赖高反射率的合作目标以保证探测信噪比。

针对这一问题，华东师范大学曾和平团队于2025年提出了一种模式可编程光频梳计算光谱方法，用于非合作目标条件下的宽带高分辨气体遥感探测[116]。如图8，该研究将二维色散系统与数字微镜器件(DMD)结合，实现了对光频梳各梳齿的独立编码，并通过单像素探测器采集后向散射信号，再计算重建目标吸收光谱。同时，结合单光子探测器，通过C_2H_2吸收光谱的测量验证了该技术可行性。

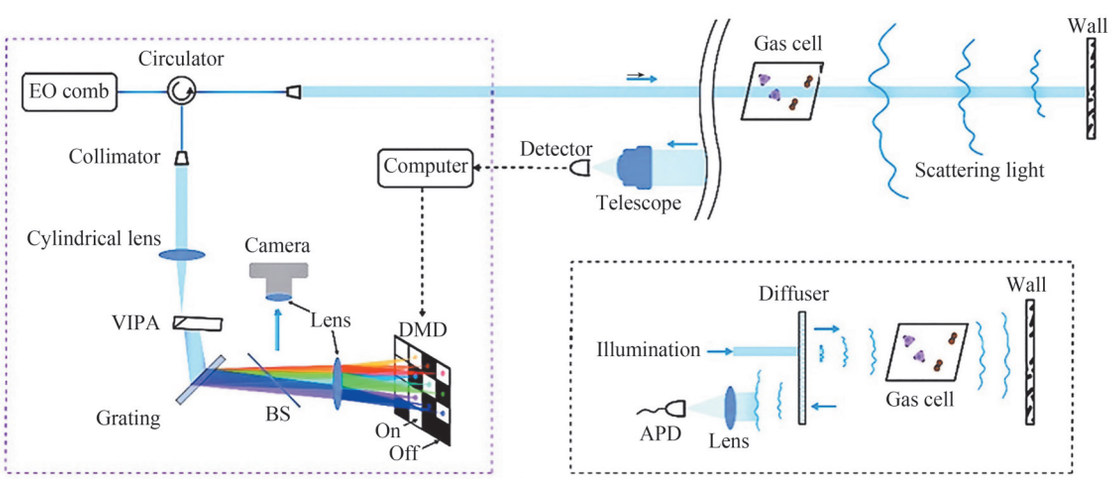

图8 可模式编程的梳状光谱技术实验装置图[116]

Fig.8 Schematic diagram of the experimental setup for mode-programmable comb spectroscopy[116]

2.2.3 路径积分扫描吸收光谱技术

为进一步提高浓度反演精度并增强对复杂大气条件的适应能力，IPAL从传统的双波长机制进一步发展为多波长机制。该方法通过连续或步进调谐激光器输出波长，获取气体吸收线上多个波长采样点数据，并结合拟合算法获取完整的气体吸收线。

在2012-2013年期间，NASA的RIRIS H等分别报道了机载CO_2和CH_4多频IPAL系统[117-118]。两套系统均通过直接调制DFB激光器实现种子光连续扫描，并在脉冲斩波和能量放大后获得目标吸收线附近约20个频率采样点，从而有效降低了系统误差，提高了柱浓度反演精度。图9(a)和(b)分别展示了CO_2多频IPAL系统结构示意图和光谱扫描结果。

除温室气体柱浓度探测外，NASA的RIRIS H等于2013年将1 529 nm扫频脉冲光源倍频至764.7 nm，用于大气中O_2柱浓度探测[119]。图9(c)和(d)分别展示了该系统的结构示意图和不同光学深度下的吸光度光谱，该系统采用单光子计数模块(SPCM-AQRH-12, Perkin Elmer)探测后向散射信号，在3～13.5 km高度范围内实现了大气柱干空气中O_2含量的精确测量。2014年，该团队进一步提升了扫描速率，并扩展至多

通道单光子探测结构，以提高计数率和时间分辨能力，同时优化滤波设置以减小谱线畸变，为ASCENDS等空基CO_2柱浓度反演提供了关键的干空气参考信息[120]。

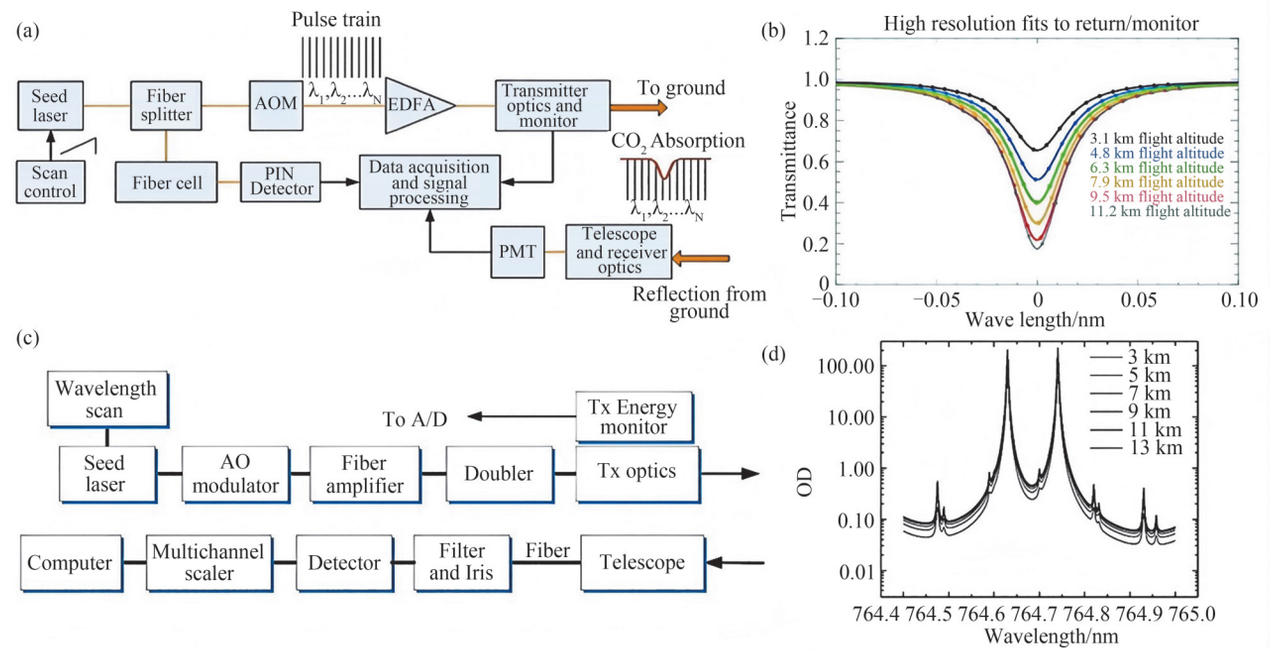

图9　NASA机载多波长IPDA激光雷达系统。(a) CO_2 IPDA激光雷达示意图；(b) 不同高度透射谱拟合线型[118]；(c) O_2 IPDA激光雷达示意图；(d) 不同高度光学深度曲线[119]

Fig.9　NASA airborne multi-wavelength IPDA lidar system. (a) Schematic of the CO_2 IPDA lidar; (b) Transmission curves at different altitudes[118]; (c) Schematic of the O_2 IPDA lidar; (d) Optical depth curves at different altitudes[119]

在以上系统中，激光频率控制方式对系统复杂度与测量精度具有决定性影响。直接通过改变激光器电流或温度进行连续扫频，具有结构简单、扫描速率快、频率点数多等优点，但同时也容易引入频率非线性误差和输出强度波动。针对这个问题，美国NIST的WAGNER G和PLUSQUELLIC D于2016年提出了一种单频外腔半导体激光器（External Cavity Diode Laser，ECDL）的快速步进频率扫描方案并构建了一套地基IPDA多种温室气体探测激光雷达[121]。该系统工作于1.6～1.65 μm波段，通过串联电光相位调制器和滤波腔进行单边带选择，在10 kHz扫描频率下实现了123个离散频率点输出，并保持各频率点近似等功率，从而减小了激光基线波动引起的系统误差。通过切换ECDL在1 602 nm和1 645 nm的中心工作波长，该系统进一步实现了单光源条件下对CO_2、H_2O和CH_4气体的路径积分浓度探测。

在工业园区、城市地下管网、矿山巷道等复杂开放环境中的气体泄漏巡检应用中，更强调遥感检测设备的小型便携化、灵活机动部署、低功率安全性和快速检测能力。在这一应用需求下，IPSAS技术虽然牺牲了距离分辨率，但对光路上易燃易爆气体探测具有很高的灵敏度，因此得到了快速发展。

2022年，英国QLM Technology Ltd的TITCHENER J等研发了基于可调谐二极管激光雷达的单光子气体成像系统，用于CH_4连续监测，如图10所示[122]。该系统融合TDLAS、DIAL与SPD技术，采用1.651 μm波段DFB激光器和InGaAs/InP SPD，实现低功率主动扫描成像。经实验室校准和现场试验验证，在10 mW激光功率输出下，可在90 m探测距离下检测低至0.012 g/s的CH_4泄漏。

2024年，中国科学院大学杭州高等研究院王建宇团队基于伪随机二进制编码的IPSAS激光雷达进行了仿真模拟，如图11所示[123]。结合高斯羽流扩散模型与Risley棱镜扫描策略，系统研究棱镜转速比、风速、泄漏率、大气稳定度、目标反射率、平均时间以及空间插值算法对泄漏率反演的影响，为后续样机参数选型和算法优化提供了定量依据。2026年，该团队验证了对CH_4定量监测的能力[124]。

2024年，韩豪彬等提出并实验验证了一种基于InGaAs/InP SPD（SPCM-1.5-M，Genius Zenith）的简易全光纤结构的IPSAS激光雷达，实现了CH_4的遥感探测，如图12所示[85]。该系统采用小型测距机用于距离探测，减小强度调制器件造成的功率损耗。对SPD中死时间、后脉冲概率、暗计数对光子计数统计进行了逐

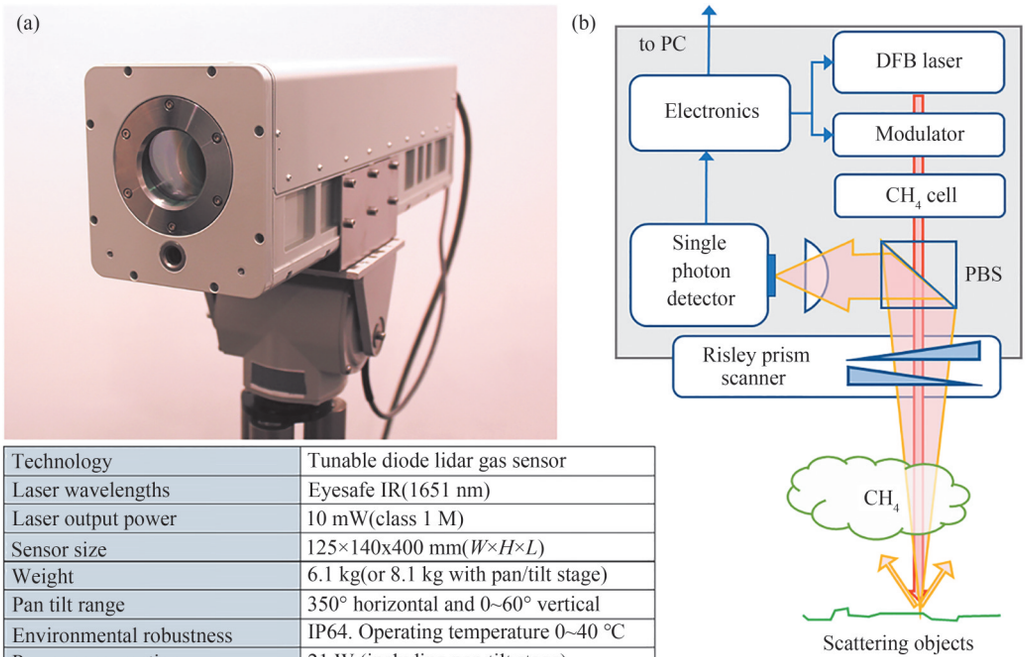

Technology	Tunable diode lidar gas sensor
Laser wavelengths	Eyesafe IR(1651 nm)
Laser output power	10 mW(class 1 M)
Sensor size	125×140x400 mm(*W*×*H*×*L*)
Weight	6.1 kg(or 8.1 kg with pan/tilt stage)
Pan tilt range	350° horizontal and 0~60° vertical
Environmental robustness	IP64. Operating temperature 0~40 ℃
Power consumption	21 W (including pan tilt stage)

图 10 基于单光子探测技术的CH_4可调谐二极管激光雷达[122]

Fig.10 Tunable diode lidar for CH_4 detection based on single-photon detection technology[122]

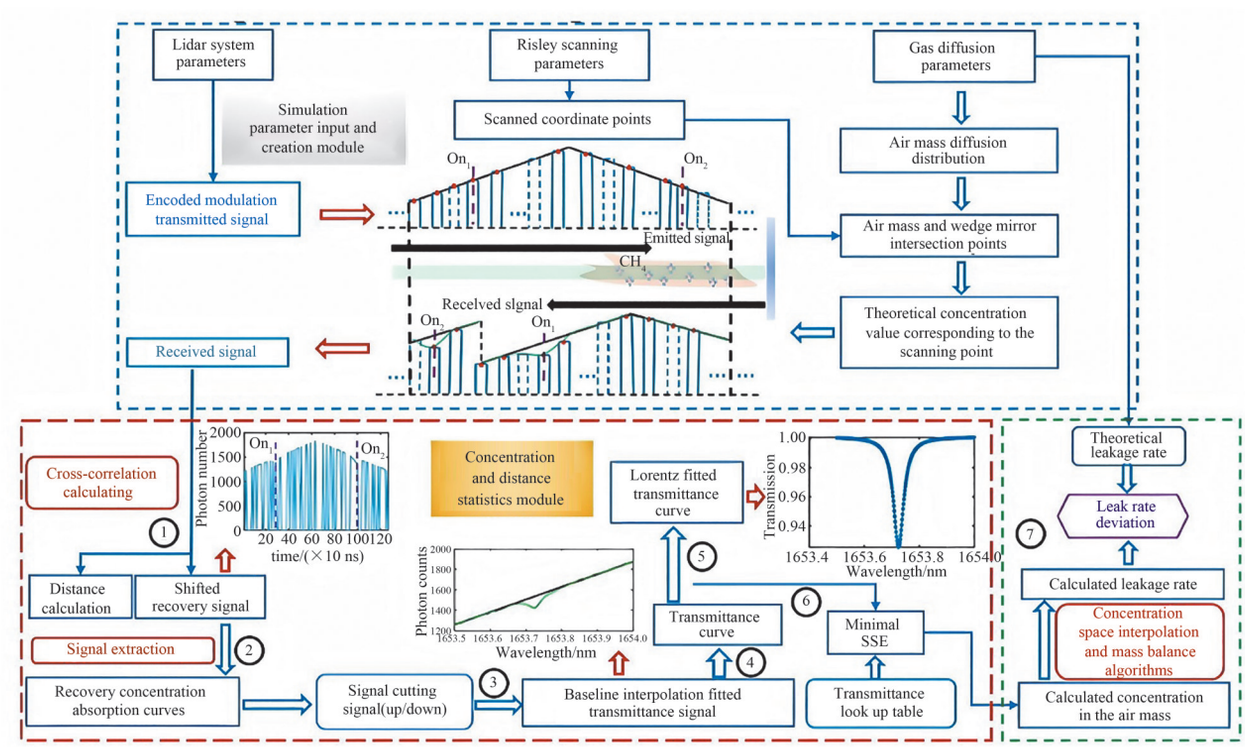

图 11 基于伪随机二进制序列编码、TDLAS和IPDA的单光子CH_4泄漏遥感方案流程图[123]

Fig.11 Flowchart of single-photon CH_4 leakage remote sensing scheme based on PRBS coding, TDLAS and IPDA[123]

一修正。采用内差探测方法和联合时频分析修正了激光器频率非线性频率误差。

2025年，费劳恩霍夫应用光子学研究中心的SMITH R等基于PPLN波导实现了UCSPD(SPCM-AQRH-16-FC, Excelitas)探测的CH_4激光雷达系统，如图13所示[125]。将1 651 nm CH_4特征波长光子上转换至798 nm后，采用Si-SPAD进行探测实现86%的内部上转换效率。然而由于耦合损耗以及泵浦噪声，系统最终的探测效率为3.47%。在户外环境中成功实现25 m处1 000 ppm·m浓度的CH_4探测。

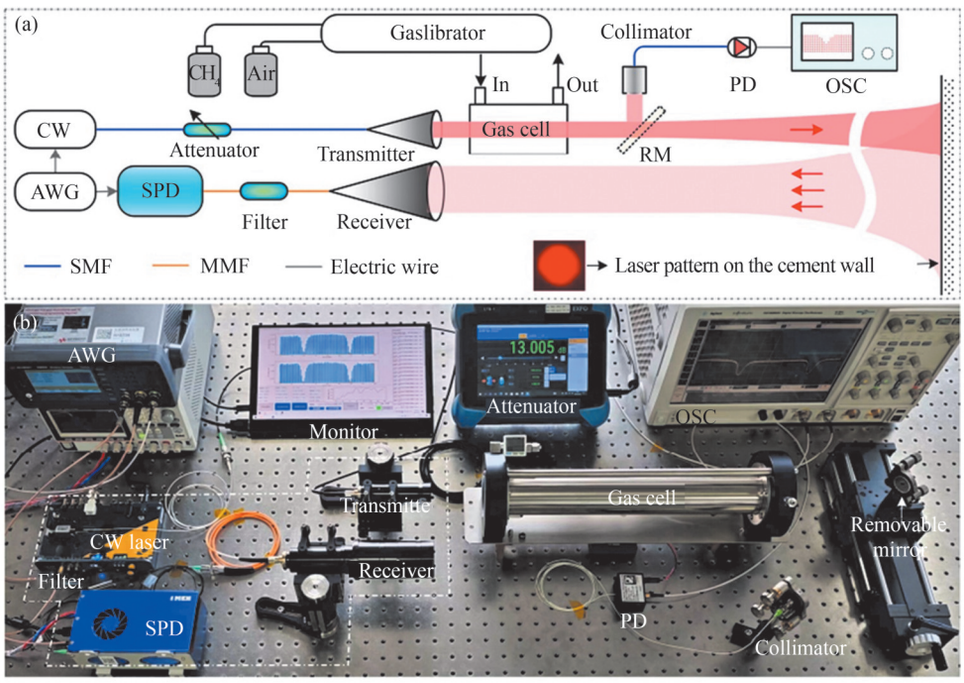

图 12　基于 InGaAs/InP SPD 的全光纤结构的 CH_4 路径积分光谱遥感系统[85]

Fig.12　All-fiber CH_4 path-integrated spectroscopic remote sensing system based on InGaAs/InP SPD[85]

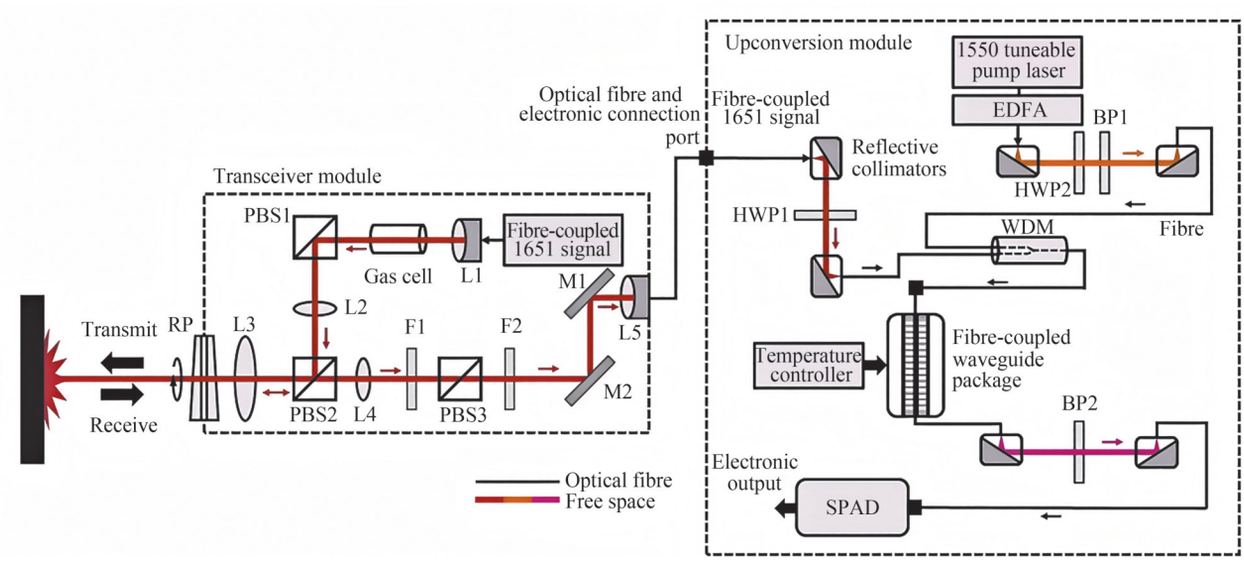

图 13　基于 UCSPD 的 CH_4 激光雷达[125]

Fig.13　CH_4 lidar based on UCSPD[125]

在化工园区、燃气输配系统、储罐区、矿井、地下空间以及复杂工业排放场景中，气体泄漏往往呈现多源并存、成分复杂、扩散迅速等特点。为解决这个问题，2025 年，韩豪彬等在原先 CH_4 单气体单光子遥感系统的基础上，采用了波长调谐范围超 100 nm 的外腔半导体二极管激光器用于覆盖 1 520～1 620 nm 波段内的气体吸收线，系统光路示意图如图 14 所示[126]。此外，配备了可编程光栅滤波器和激光出射波长同步调谐，实现不同探测频率下对背景光的滤波，提高系统在强背景光下的连续工作能力。通过对波长跨度为 45 nm 的 NH_3、C_2H_2、$H^{13}CN$ 和 CO 四种气体进行探测验证了系统在多气体遥感探测中的能力。

为了提高多气体遥感系统的气体识别速率，郭可欣等于 2026 年提出并验证了基于时域重叠光谱的可重构光路路径积分光谱单光子激光雷达系统[86]。该系统采用异步触发机制并结合 InGaAs/InP SPD（SPCM-1.5-M，Genius Zenith）的高灵敏度，在 10 μs 单扫描周期内完成 $H^{13}CN$、CO、C_2H_2、CH_4 四种气体的同时扫描。

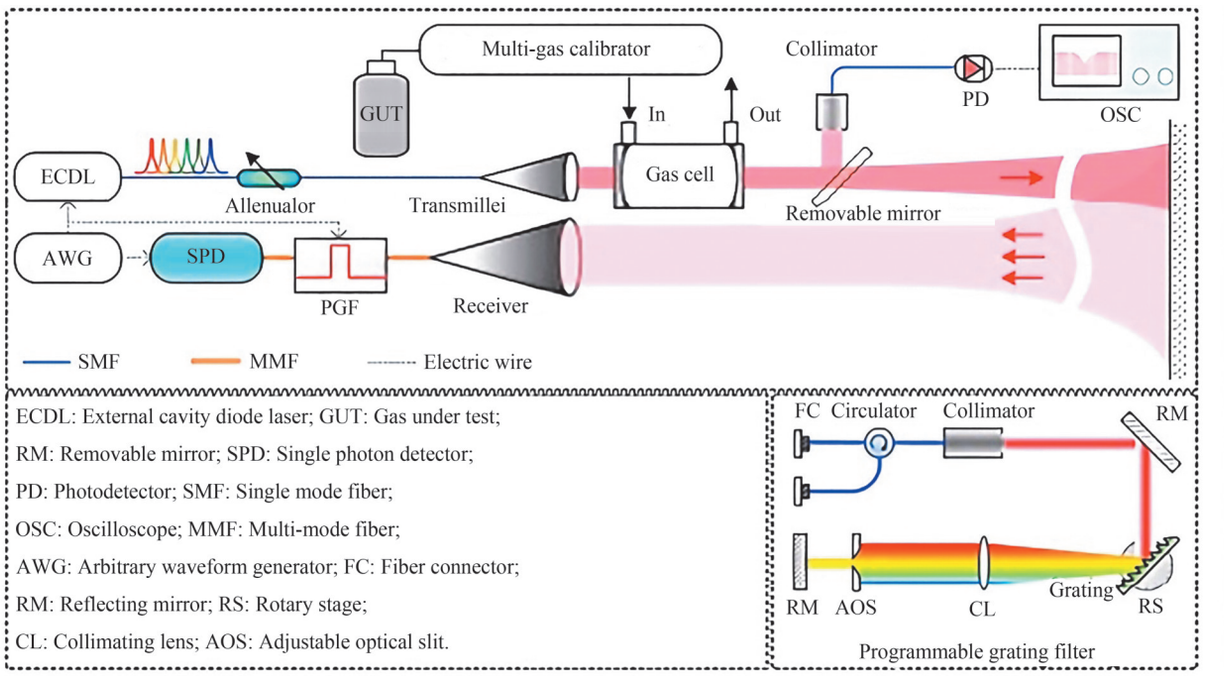

图 14 多气体泄漏监测路径积分光谱单光子激光雷达的实验系统结构示意图，以及可编程光栅滤波器的内部示意图（右下角插图）[126]

Fig.14 Schematic of the experimental system for multi-gas leakage monitoring path-integrated spectroscopic single photon lidar, with inset (bottom right) showing the internal structure of the programmable grating filter[126]

并通过可编程光栅滤波器实现多频率通带窄带带通滤波，以满足白天等强背景光下多气体同时识别的能力。此外，系统仅对已识别到的气体逐一精细分析，避免了对未泄漏气体重复扫描导致的时间损耗。图 15 展示了基于时域堆叠光谱的多气体同时识别遥感系统。

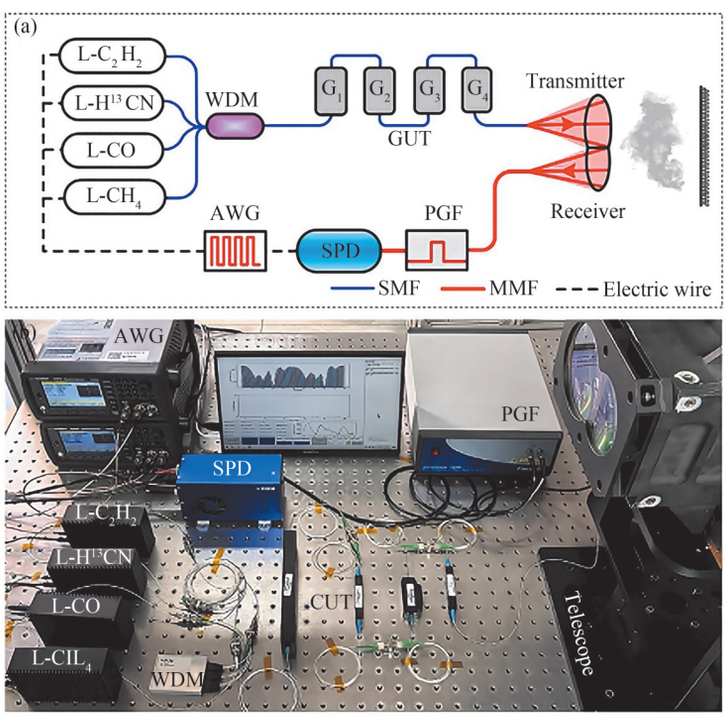

图 15 基于时域堆叠光谱技术的可重构光路路径积分光谱单光子激光雷达[86]。(a)光路图；(b)实物图

Fig.15 Reconfigurable optical path single-photon path-integrated spectroscopic single photon lidar based on time-domain over-lapping spectroscopy[86]. (a) Schematic of optical path; (b) Photograph of the experimental setup

2.3 差分吸收光谱激光雷达

DIAL具备距离分辨的能力，但不具备光谱分辨率；IPAL具备光谱分辨率但没有距离分辨率；而DASL同时具有距离分辨率和光谱分辨率。

2021年，中国科学技术大学余赛芬等采用SNSPD实现了单光子探测的DASL，对近红外波段多气体有距离分辨率的高光谱分辨遥感[50]。系统光路如图16(a)所示，首先，采用光频梳拍频锁定技术，实现探测激光在百纳米光谱范围内的精确波长锁定，可实现多种气体的同时分析。其次，不再依赖提高激光器功率和扩大望远镜面积，而是研制了高效率、低噪声、大面元的SNSPD，提高了激光雷达探测信噪比。最后，提出实时补偿技术，通过高速切换、交替发射探测激光和参考激光，实时校正大气气溶胶变化、湍流影响望远镜接收效率、出射激光功率漂移、探测器效率变化等因素。系统采用30组探测激光和参考激光时分复用，相当于集成了30套双波长差分吸收激光雷达（即在探测时序上每一个探测波长后都会紧跟一个参考波长）。该工作以CO_2和半重水（HDO）遥感分析为例，实现了有距离分辨的大气光谱精确分析。如图16(b)所示，在光谱分析范围内，包含了1条CO_2吸收线和2条HDO吸收线，重叠吸收深度随距离递增。HDO在大气中的自然丰度仅约为H_2O的1/3 200，常被忽略。通过三峰拟合可以同时提取出CO_2和HDO吸收光谱。在4 km距离处的实测光谱中，CO_2主峰与两个HDO弱峰被清晰地分离出来，其浓度反演不确定度为±14.3%。该系统采用9像素大口径（200 μm直径）多模SNSPD（总量子效率31.5%），降低了湍流对自由空间到光纤的耦合效率影响。

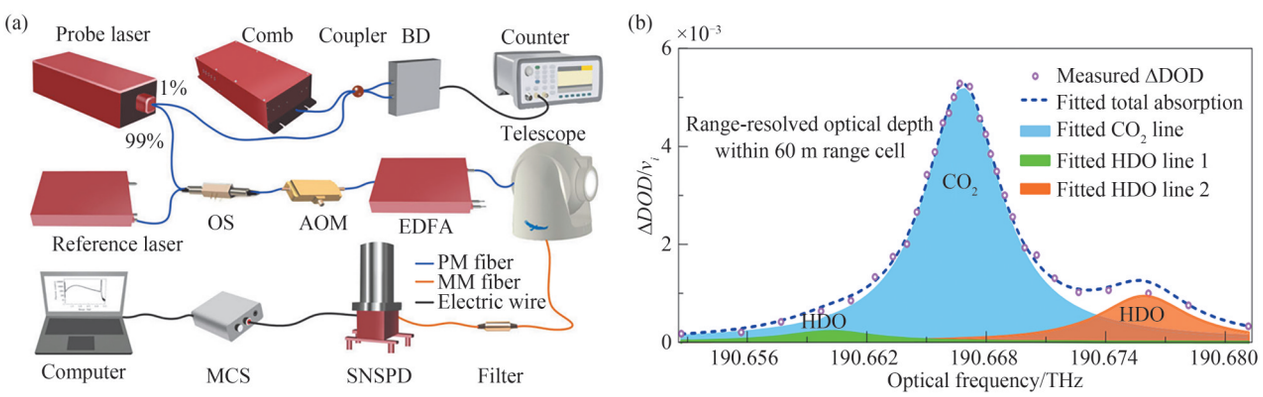

图16 CO_2 DASL实验装置与距离分辨光谱拟合结果图[50]。(a) 系统示意图；(b) 60 m距离分辨单元内CO_2与HDO气体吸收线的洛伦兹拟合光谱

Fig.16 Experimental setup and range-resolved gas absorption spectral fitting of CO_2 differential absorption spectroscopy lidar[50]. (a) Schematic of the system; (b) Lorentzian-fitted absorption spectra of CO_2 and HDO within a 60 m range-resolution cell

在2025-2026年期间，为了进一步证明DASL对多种气体探测的能力，该团队开展了系列理论研究[127-128]。针对1.5 μm波段优选低温度敏感性吸收线，系统地评估了温度、压力、激光频率等误差源的影响。采用30个非均匀采样波长，精准反演$H_2{}^{16}O$、$HD^{16}O$廓线及其同位素比值δD。同时基于MODTRAN模型，完成了CO_2与$HD^{16}O$的同步遥感敏感性分析，验证了R16谱线的适用性，明确了大气参数、激光频移及光谱重叠对反演结果的影响。实现了对流层内CO_2与$HD^{16}O$的高精度距离分辨浓度反演，为多种气体的高时空分辨遥感提供了理论基础与可行性分析。

在实际的气体遥感监测中，根据具体的应用场景与探测需求，DIAL、IPAL以及DASL各具优势。具有距离分辨率的DIAL系统通常用于对中尺度区域的气体浓度分布监测与大气成分剖面分析。IPAL通常用于：1)机载与星载遥感平台进行大空间尺度遥感探测，满足高时间分辨率需求；2)复杂环境中进行快速气体泄漏检测。而针对复杂科研任务，传统单一的功能特点难以兼顾多光谱识别与高时空分辨率，DASL同时具备距离分辨与连续光谱扫描能力，并能够实现在开放光路下的多组分气体同时探测。针对单光子探测技术在不同气体遥感探测机制中的应用进行了总结，如表2所示。

表2 单光子探测技术在不同气体遥感探测机制中的应用

Table 2 Application of single-photon detection technology in various remote sensing mechanisms for gas detection

Detection principle	Spectral resolution	Spatial resolution	Temporal resolution	Target gas	Detection error	References
DIAL	×	500 m	5 min	CO_2	＜2%（5.2 km）	[95]§
		150 m	10 min	H_2O	＜10%（2.5 km）	[96]-*
		250 m	10 min	CO_2, H_2O	0.5%、4%（1 km）	[97]§
		200 m	15 min	CH_4	＜11%（3～9 km）	[98]§
		150 m	15 s	CO_2	～2.1%（2 km）	[46]-
		250 m	10 min	CO_2, CH_4, H_2O	1～2%（DIAL）	[100]-
		30 m	5 min	CO_2	2.3%	[101]-
		25 m	15 min	CO_2	≤6.8%（0.7 km）	[102]-
IPAL	IPDA	√	×	7 s	CO_2	0.67%	[107]§
	IPDCS			15 min	CO_2, H_2O, HDO	NA	[115]
				NA	C_2H_2	0.7%	[116]*
				1 s	CH_4	0.33%	[117]*
				0.9 s	CO_2	≤0.23%（8～10 km）	[118]§
				1 s	O_2	2-3%	[119]*
				10 s	O_2	2.5%	[120]*
				30 s	CO_2, CH_4	0.7%, 1.2%	[121]-*
	IPSAS			0.01 s	CH_4	10%	[122]#
				1 s	CH_4	0.46%	[85]#
				0.01 s	CH_4	NA	[125]
				1 s	CO, $H^{13}CN$ C_2H_2, NH_3	0.13%, 0.13% 0.02%, 0.17%	[126]#
				1 s	C_2H_2, $H^{13}CN$ CO, CH_4	0.43%（C_2H_2） 0.48%（CH_4）	[86]#
DASL	0.5 MHz	60 m	10 min	CO_2, HDO	1.2%, 14.3%	[50]-

#实测结果与标准气体腔浓度对比；-雷达与原位仪器对比；*雷达测试与模拟结果对比；§根据实验数据信噪比进行误差估计

3 总结与展望

结合国内外研究进展，近红外单光子技术突破了传统红外气体遥感回波信号微弱、探测器灵敏度不足的瓶颈，实现了从常规模拟光电探测到数字化单光子精密探测的进步，推动高精度、远距离大气气体遥感和应用。在具体考虑使用哪种技术手段时，除了分辨率需求（光谱、空间、时间）和气体探测种类，探测精度也是重要的考量指标。传统气体探测激光雷达的误差根据来源分为五类：1）系统探测误差；2）光学参量振荡频率变换不稳定性引入的误差；3）底层光谱数据库与谱线线型模型的偏差；4）气象传感数据的误差；5）积分时间内，温压廓线的变化引起的误差[97]。而采用单光子探测系统，可以弱化对激光器功率的需求，采用脉冲能量小但重复频率高的全光纤激光器或小型化玻璃激光器，避免光学频率变换不稳定性。

面向“双碳”战略对温室气体高精度监测的迫切需求，以及工业安全、城市环境治理对痕量气体泄漏快速响应的现实要求，近红外单光子气体遥感技术仍然存在需要解决的问题，在室温工作条件下的暗计数率与后脉冲概率仍制约着探测器的探测极限，实现高灵敏度与系统结构小型化之间的矛盾没有根本解决，面向多场景部署的系统稳定性还需要验证。展望未来，近红外单光子探测技术在气体遥感应用的发展可从以下四个方面展开叙述：

1）基于单光子探测技术的气体遥感激光雷达的精度主要依赖光子计数。目前激光脉冲能量不断提高，导致近场信号造成单光子探测器计数饱和。因此，为了节省累积时间，需要提高探测器的最大计数率。

2）从应用出发，需要提高系统的集成度和稳定性。当前，单光子气体探测激光雷达处在原理验证和科学研究的应用阶段。采用单光子探测的优势在于可以避免采用复杂光学结构、大功率的激光器和大口径望

远镜。然而，SNSPD和UCSPD自身的复杂度和稳定性仍是亟待解决的挑战，且运行成本高，限制了这类探测器的广泛应用。InGaAs/InP SPD的挑战性在于不断优化材料和工艺结构、电子学设计和校准方法，以提高其综合性能。无论哪种途径，高量子效率、高饱和计数率、大面元、低噪声的单光子探测器是激光雷达遥感的理想追求。

3）单光子探测激光雷达在多气体遥感探测上进一步发展。当前，多气体探测仍以原位探测为主，难以满足大范围、实时、遥测一体化的应用需求。急需推动单光子激光雷达从单一气体探测向多组分气体同时探测发展，解决多波长并行探测、低串扰信号提取和多光谱数据融合等关键技术。

4）中红外波段（3～5 μm、8～12 μm）的气体吸收线相比近红外和可见光波段更加丰富，且气体分子在该波段的吸收强度更大，从而提高了该波段的灵敏度[129-130]。因此，未来的气体遥感系统应拓展到中红外波段，进一步提升对目标气体的探测能力。这需要开发新的激光光源和单光子探测器，特别是具有宽光谱调谐范围的中红外激光器，以及在中红外波段具有高探测效率、低暗计数率和较低后脉冲的单光子探测器。这些技术的突破将进一步提升激光雷达在工业安全监测、环境污染防控及公共健康保障等领域的应用价值。

参考文献

[1] WU Hao, WANG Yingyu, SUN Shiyi, et al. Performance bounds of ranging precision in SPAD-based dTOF lidar[J]. Sensors, 2025, 25(19): 6184.

[2] LI Haochen, ZHENG Kaiming, GE Rui, et al. Noise-tolerant lidar approaching the standard quantum-limited precision [J]. Light: Science & Applications, 2025, 14(1): 138.

[3] DENG Yuwang, LIU Jun, XIAO Hailong, et al. Developments in atmospheric remote sensing lidar based on single-photon detection[J]. Laser & Optoelectronics Progress, 2025, 62(10): 1000002.
邓雨旺, 刘钧, 肖海龙, 等. 基于单光子探测技术的大气遥感激光雷达发展现状[J]. 激光与光电子学进展, 2025, 62(10): 1000002.

[4] YUAN Jinlong, SU Lian, XIA Haiyun, et al. Microburst, windshear, gust front, and vortex detection in mega airport using a single coherent Doppler wind lidar[J]. Remote Sensing, 2022, 14(7): 1626.

[5] WEI Tianwen, XIA Haiyun, WU Kenan, et al. Dark/bright band of melting layer detected by coherent Doppler lidar and micro rain radar[J]. Optics Express, 2022, 30(3): 3654-3664.

[6] YUAN Jinlong, XIA Haiyun, WEI Tianwen, et al. Identifying cloud, precipitation, windshear, and turbulence by deep analysis of power spectrum of coherent Doppler wind lidar[J]. Optics Express, 2020, 28(25): 37406-37418.

[7] XIA Haiyun, CHEN Yixiang, YUAN Jinlong, et al. Windshear detection in rain using a 30 km radius coherent Doppler wind Lidar at mega airport in Plateau[J]. Remote Sensing, 2024, 16(5): 924.

[8] SU Lian, LU Chunsong, YUAN Jinlong, et al. Measurement report: the promotion of low-level jet and thermal-effect on development of deep convective boundary layer at the southern edge of the Taklimakan Desert[J]. Atmospheric Chemistry and Physics, 2024, 24: 10947-10963.

[9] CHEN Anning, YUAN Jinlong, YANG Haoyu, et al. Identification and forecasting of low-level wind shear based on long range Doppler wind lidar[J]. Atmospheric Research, 2026, 330: 108558.

[10] TANG Dawei, LI Zhekai, XIA Haiyun. Clustering of weak fluorescence spectra from bioaerosol in air using laser-induced fluorescence lidar[J]. Optics Express, 2025, 33(12): 24396-24412.

[11] JIANG Pu, XIA Haiyun, HU Jiadong, et al. Estimation of atmospheric refractive index structure constant using an InGaAs/InP single-photon detector[J]. Optics Letters, 2023, 48(23): 6104.

[12] SHANGGUAN Mingjia, XIA Haiyun, WANG Chong, et al. Dual-frequency Doppler lidar for wind detection with a superconducting nanowire single-photon detector[J]. Optics Letters, 2017, 42(18): 3541.

[13] QIU Jiawei, XIA Haiyun, SHANGGUAN Mingjia, et al. Micro-pulse polarization lidar at 1.5 μm using a single superconducting nanowire single-photon detector[J]. Optics Letters, 2017, 42(21): 4454.

[14] LI Manyi, WU Yunbin, YUAN Jinlong, et al. Stratospheric aerosol lidar with a 300 μm diameter superconducting nanowire single-photon detector at 1 064 nm[J]. Optics Express, 2023, 31(2): 2768.

[15] XIA Haiyun, GUO Shentu, SHANGGUAN Mingjia, et al. Long-range micro-pulse aerosol lidar at 15 μm with an upconversion single-photon detector[J]. Optics Letters, 2015, 40(7): 1579.

[16] SHANGGUAN Mingjia, XIA Haiyun, WANG Chong, et al. All-fiber upconversion high spectral resolution wind lidar using a Fabry-Perot interferometer[J]. Optics Express, 2016, 24(17): 19322.

[17] GIBSON A J, THOMAS L. Ultraviolet laser sounding of the troposphere and lower stratosphere[J]. Nature, 1975, 256(5518): 561-563.

[18] MÉGIE G, ALLAIN J Y, CHANIN M L, et al. Vertical profile of stratospheric ozone by lidar sounding from the ground [J]. Nature, 1977, 270(5635): 329-331.

[19] WU Yonghua, YU Guming, HU Huanling, et al. D_2 stimulated raman scattering pumped by fourth harmonic Nd:YAG laser and its application in laser radar[J]. Chinese Journal of Lasers, 2000, 27(9): 824-827.
吴永华, 岳古明, 胡欢陵, 等. Nd:YAG四倍频激光抽运氘后的拉曼效应及其在激光雷达中的应用[J]. 中国激光, 2000, 27(9): 824-827.

[20] MCDERMID I S, BEYERLE G, HANER D A, et al. Redesign and improved performance of the tropospheric ozone lidar at the Jet Propulsion Laboratory Table Mountain Facility[J]. Applied Optics, 2002, 41(36): 7550.

[21] SULLIVAN J T, MCGEE T J, SUMNICHT G K, et al. A mobile differential absorption lidar to measure sub-hourly fluctuation of tropospheric ozone profiles in the Baltimore-Washington, D.C. region[J]. Atmospheric Measurement Techniques, 2014, 7(10): 3529-3548.

[22] GRANADOS-MUÑOZ M J, LEBLANC T. Tropospheric ozone seasonal and long-term variability as seen by lidar and surface measurements at the JPL-Table Mountain Facility, California[J]. Atmospheric Chemistry and Physics, 2016, 16(14): 9299-9319.

[23] DE YOUNG R, CARRION W, GANOE R, et al. Langley mobile ozone lidar: ozone and aerosol atmospheric profiling for air quality research[J]. Applied Optics, 2017, 56(3): 721.

[24] ZHAO Yirui, CAO Nianwen, JIA Pengcheng, et al. Simultaneous observation of ozone and aerosol via ultraviolet multi-wavelength lidar[J]. Laser & Optoelectronics Progress, 2022, 59(16): 1601001.
赵忆睿, 曹念文, 贾鹏程, 等. 紫外多波长激光雷达的臭氧和气溶胶同步观测研究[J]. 激光与光电子学进展, 2022, 59(16): 1601001.

[25] ZHAO Xiansong, YU Chao, WANG Chong, et al. Differential absorption ozone lidar with 4H-SiC single-photon detectors[J]. Applied Physics Letters, 2024, 125(21): 211103.

[26] JI Jie, XIE Chenbo, CHEN Jianfeng, et al. A selective review of ozone differential absorption lidar systems[J]. Optics & Laser Technology, 2026, 195: 114603.

[27] MELFI S H, LAWRENCE J D, MCCORMICK M P. Observation of raman scattering by water vapor in the atmosphere[J]. Applied Physics Letters, 1969, 15(9): 295-297.

[28] WHITEMAN D N, MELFI S H, FERRARE R A. Raman lidar system for the measurement of water vapor and aerosols in the Earth's atmosphere[J]. Applied Optics, 1992, 31(16): 3068.

[29] ANSMANN A, RIEBESELL M, WANDINGER U, et al. Combined raman elastic-backscatter lidar for vertical profiling of moisture, aerosol extinction, backscatter, and lidar ratio[J]. Applied Physics B, 1992, 55(1): 18-28.

[30] SHAEFER J, SCHREMS O, BEYERLE G, et al. Modular and mobile multipurpose lidar system for observation of tropospheric and stratospheric aerosols[C]. Lidar Techniques for Remote Sensing II: Vol. 2581. SPIE, 1995: 128-136.

[31] GOLDSMITH J E M, BLAIR F H, BISSON S E, et al. Turn-key Raman lidar for profiling atmospheric water vapor, clouds, and aerosols[J]. Applied Optics, 1998, 37(21): 4979.

[32] SHERLOCK V, GARNIER A, HAUCHECORNE A, et al. Implementation and validation of a Raman lidar measurement of middle and upper tropospheric water vapor[J]. Applied Optics, 1999, 38(27): 5838.

[33] BEHRENDT A, NAKAMURA T, ONISHI M, et al. Combined Raman lidar for the measurement of atmospheric temperature, water vapor, particle extinction coefficient, and particle backscatter coefficient[J]. Applied Optics, 2002, 41(36): 7657-7666.

[34] SAKAI T, NAGAI T, NAKAZATO M, et al. Raman lidar measurement of water vapor and ice clouds associated with Asian dust layer over Tsukuba, Japan[J]. Geophysical Research Letters, 2004, 31(6): 2003GL019332.

[35] LEBLANC T, MCDERMID I S, WALSH T D. Ground-based water vapor raman lidar measurements up to the upper troposphere and lower stratosphere for long-term monitoring[J]. Atmospheric Measurement Techniques, 2012, 5(1): 17-36.

[36] WANG Yufeng, GAO Fei, ZHU Chengxuan, et al. Raman lidar for atmospheric temperature, humidity and aerosols up to troposphere height[J]. Acta Optica Sinica, 2015, 35(3): 0328004.
王玉峰, 高飞, 朱承炫, 等. 对流层高度大气温度、湿度和气溶胶的拉曼激光雷达系统[J]. 光学学报, 2015(3): 0328004.

[37] CHU Yufei, LIU Dong, WU Decheng, et al. Algorithm of retrieving boundary layer height based on raman lidar water vapor data[J]. Chinese Journal of Lasers, 2020, 47(12): 1204009.
储玉飞, 刘东, 吴德成, 等. 基于拉曼激光雷达水汽数据探测边界层高度的算法[J]. 中国激光, 2020, 47(12): 1204009.

[38] LIU Fuchao, YI Fan, HE Yun, et al. Spectrally resolved raman lidar to measure backscatter spectra of atmospheric three-phase water and fluorescent aerosols simultaneously: instrument, methodology, and preliminary results[J]. IEEE Transactions on Geoscience and Remote Sensing, 2022, 60: 1-13.

[39] HUANG Yisen, BU Lingbing, YANG Bin, et al. Retrieval and validation of atmospheric boundary layer height based on temperature and humidity raman lidar[J]. Laser & Optoelectronics Progress, 2025, 62(21): 2101002.
黄驿森, 卜令兵, 杨彬, 等. 基于温湿拉曼激光雷达反演大气边界层高度的方法与验证[J]. 激光与光电子学进展,

2025(21):2101002.
[40] HU Shunxing, CHEN Yafeng, LIU Qiuwu, et al. Differential absorption lidar system for background atmospheric so_2 and no_2 measurements[J]. Chinese Journal of Lasers, 2018, 45(9): 0911009.
胡顺星, 陈亚峰, 刘秋武, 等. 差分吸收激光雷达系统探测背景大气SO_2和NO_2[J]. 中国激光, 2018, 45(9): 0911009.
[41] FREDRIKSSON K, GALLE B, NYSTROM K, et al. Mobile lidar system for environmental probing[J]. Applied Optics, 1981, 20(24): 4181.
[42] DU Zhenhui, ZHANG Shuai, LI Jinyi, et al. Mid-infrared tunable laser-based broadband fingerprint absorption spectroscopy for trace gas sensing: a review[J]. Applied Sciences. 2019, 9(2):338.
[43] KIZILKAN E. Advanced silicon and SWIR single-photon avalanche diodes: design, simulation, and characterization[D]. Lausanne: Ecole Polytechnique Federale de Lausanne, 2024.
[44] VANDEVENDER A P, KWIAT P G. High efficiency single photon detection via frequency up-conversion[J]. Journal of Modern Optics, 2004, 51(9-10): 1433-1445.
[45] TSMAN G NGOL, OKUNEV O, CHULKOVA G, et al. Picosecond superconducting single-photon optical detector [J]. Applied Physics Letters, 2001, 79(6): 705-707.
[46] YUE Bin, YU Saifen, LI Mangyi, et al. Local-scale horizontal CO_2 flux estimation incorporating differential absorption lidar and coherent doppler wind lidar[J]. Remote Sensing, 2022, 14(20): 5150.
[47] YU Chao, SHANGGUAN Mingjia, XIA Haiyun, et al. Fully integrated free-running InGaAs/InP single-photon detector for accurate lidar applications[J]. Optics Express, 2017, 25(13): 14611-14620.
[48] YU Chao, QIU Jiawei, XIA Haiyun, et al. Compact and lightweight 1.5μm lidar with a multi-mode fiber coupling free-running InGaAs/InP single-photon detector[J]. Review of Scientific Instruments, 2018, 89(10): 103106.
[49] XIA Haiyun, SHANGGUAN Mingjia, WANG Chong, et al. Micro-pulse upconversion Doppler lidar for wind and visibility detection in the atmospheric boundary layer[J]. Optics Letters, 2016, 41(22): 5218-5221.
[50] YU Saifen, ZHANG Zhen, XIA Haiyun, et al. Photon-counting distributed free-space spectroscopy[J]. Light Science & Applications, 2021, 10: 212.
[51] MARSILI F, VERMA V B, STERN J A, et al. Detecting single infrared photons with 93% system efficiency[J]. Nature Photonics, 2013, 7(3): 210-214.
[52] ABSHIRE J B, RAMANATHAN A K, RIRIS H, et al. Airborne measurements of CO_2 column concentrations made with a pulsed IPDA lidar using a multiple-wavelength-locked laser and HgCdTe APD detector[J]. Atmospheric Measurement Techniques, 2018, 11: 2001-2025.
[53] SUN X, ABSHIRE J B, RAMANATHAN A, et al. Retrieval algorithm for the column CO_2 mixing ratio from pulsed multi-wavelength lidar measurements[J]. Atmospheric Measurement Techniques, 2021, 14: 3909-3922.
[54] MAO J, ABSHIRE J B, KAWA S R, et al. Airborne lidar measurements of atmospheric CO_2 column concentrations to cloud tops made during the 2017 ASCENDS/ABoVE campaign[J]. Atmospheric Measurement Techniques, 2024, 17: 1061-1074.
[55] WANG J S, KAWA S R, ELUSZKIEWICZ J, et al. A regional CO_2 observing system simulation experiment for the ASCENDS satellite mission[J]. Atmospheric Chemistry and Physics, 2014, 14: 12897-12914.
[56] EHRET G, BOUSQUET P, PIERANGELO C, et al. MERLIN: a French-German space lidar mission dedicated to atmospheric methane[J]. Remote Sensing, 2017, 9(10): 1052.
[57] PIERANGELO C, MILLET B, ESTEVE F, et al. Merlin (methane remote sensing lidar mission): an overview[C]. EPJ Web of Conferences, 2016, 119: 26001.
[58] AMEDIEK A, EHRET G, FIX A, et al. CHARM-F—a new airborne integrated-path differential-absorption lidar for carbon dioxide and methane observations: measurement performance and quantification of strong point source emissions [J]. Applied Optics, 2017, 56(18): 5182-5197.
[59] FIX A, BÜDENBENDER C, WIRTH M, et al. Optical parametric oscillators and amplifiers for airborne and spaceborne active remote sensing of CO_2 and CH_4[C]. Lidar technologies, techniques, and measurements for atmospheric remote sensing VII, 2011, 8182: 28-37.
[60] DI Huige, LI Xiao, HUA Dengxin, et al. Research status and progress of lidar for atmosphere in China[J]. Microw Opt Technol Lett, 2021, 63: 2129-2134.
[61] CHEN Weibiao, LIU Jiqiao, HOU Xia, et al. Lidar technology for atmosphere environment monitoring satellite[J]. Aerospace Shanghai (Chinese & English), 2023, 40(3): 13-20.
陈卫标, 刘继桥, 侯霞, 等. 大气环境监测卫星激光雷达技术[J]. 上海航天(中英文), 2023, 40(3): 13-20.
[62] FAN Chuncan, CHEN Cheng, LIU Jiqiao, et al. Preliminary analysis of global column-averaged CO_2 concentration data from the spaceborne aerosol and carbon dioxide detection lidar onboard AEMS[J]. Optics Express, 2024 , 32(12): 21870-21886.
[63] ZHANG Hongyuan, HAN Ge, CHEN Weibiao, et al. Validation Method for Spaceborne IPDA LIDAR XCO_2 Products via

TCCON[J]. IEEE Journal of Selected Topics in Applied Earth Observations and Remote Sensing, 2024, 17: 16984-16992.
[64] LIN Hongze, WU Kaihua, ZHANG Ting, et al. Remote sensing of vehicle emitted carbon oxides employing wavelength modulation spectroscopy and a segment modulation method[J]. Microwave and Optical Technology Letters, 2023, 65(7): 1162-1168.
[65] CHENG Yuan, YU Jiheng, KONG Zheng, et al. Diode-laser based field deployable continuous-wave differential absorption lidar for atmospheric NO_2 monitoring[J]. Optics and Lasers in Engineering, 2024, 181: 108344.
[66] YU Jiheng, CHENG Yuan, KONG Zheng, et al. Broadband continuous-wave differential absorption lidar for atmospheric remote sensing of water vapor[J]. Optics Express, 2024, 32(3): 3046-3061.
[67] GONG Wei, XIANG Chengzhi, MAO Feiyue, et al. Wavelet modulus maxima method for on-line wavelength location of pulsed lidar in CO_2 differential absorption lidar detection[J]. Photonics Research, 2016, 4(2): 020074.
[68] YANG Keyi, HAN Ge, MAO Huiqin, et al. High-resolution XCH_4 anomaly detection method using GF-5 AHSI payload [J]. Journal of Atmospheric and Environmental Optics, 2022, 17(6): 670-678.
[69] HAN Ge, HUANG Yiyang, SHI Tianqi, et al. Quantifying CO_2 emissions of power plants with Aerosols and Carbon Dioxide Lidar onboard DQ-1[J]. Remote Sensing of Environment, 2024, 313: 114368.
[70] YANG Keyi, HAN Ge, HE Hu, et al. Analysis of temporal variations in oilfield methane emissions based on multi-source domestic hyperspectral satellites[J]. National Remote Sensing Bulletin, 2026, 30(3): 623-634.
[71] WANG Shuaibo, JU Ke, CHEN Sijie, et al. Performance evaluation of spaceborne integrated path differential absorption lidar for carbon dioxide detection at 1572 nm[J]. Remote Sensing, 2020, 12(16): 2570.
[72] WANG Shuaibo, XU Wentao, CHEN Sijie, et al. Synergistic monitoring of PM2.5 and CO_2 based on active and passive remote sensing fusion during the 2022 Beijing Winter Olympics[J]. Applied Optics, 2024, 63(5): 1231-1240.
[73] WANG Shuaibo, CHENG Chonghui, CHEN Sijie, et al. Development of China's atmospheric environment monitoring satellite CO_2 IPDA lidar retrieval algorithm based on airborne campaigns[J]. Remote Sensing of Environment, 2024, 315: 114473.
[74] CHENG Chonghui, LIU Dong, WANG Shuaibo, et al. Estimating strong point CO_2 emissions by combining spaceborne IPDA lidar and HSRL[J]. Remote Sensing of Environment, 2025, 328: 114898.
[75] HU Shunxing, HU Huanling, WU Yonghua, et al. L625 differential absorption lidar system for tropospheric ozone measurements[J]. Acta Optica Sinica, 2004, 24(5): 597-601.
胡顺星, 胡欢陵, 吴永华, 等. L625差分吸收激光雷达探测对流层臭氧[J]. 光学学报, 2004, 24(5): 597-601.
[76] LIU Qiuwu, CHEN Yafeng, WANG Jie, et al. Detection of atmospheric NO_2 concentration by differential absorption lidar based on dye lasers[J]. Acta Optica Sinica, 2017, 37(4): 0428004.
[77] MA Hui, LIU Dong, LI Wenfeng, et al. A rapid and accurate optimizing algorithm for IPDA lidar data inversion[J]. Spectroscopy and Spectral Analysis, 2018, 38(4): 1014-1018.
[78] TIAN Xiaomin, MA Hui, LIU Dong, et al. Optimized weighting function for IPDA lidar concerning the lower layer CO_2 concentration fluctuation[J]. Journal of Quantitative Spectroscopy & Radiative Transfer, 2019, 224: 120-124.
[79] XING Chenzhi, LIU Cheng, WANG Shanshan, et al. Observations of the vertical distributions of summertime atmospheric pollutants and the corresponding ozone production in Shanghai, China[J]. Atmospheric Chemistry and Physics, 2017, 17: 14275-14289.
[80] ZHANG Chengxin, LIU Cheng, CHAN Ka Lok, et al. First observation of tropospheric nitrogen dioxide from the Environmental Trace Gases Monitoring Instrument onboard the GaoFen-5 satellite[J]. Light Science and Applications, 2020, 9: 66.
[81] YUAN Tian, LIU Cheng, SUN Youwen, et al. Satellite observations reveal a large CO emission discrepancy from industrial point sources over China[J]. Geophysical Research Letters, 2022, 49: 097312.
[82] ZHAO Fei, LIU Cheng, HU Qihou, et al. High spatial resolution ozone profiles retrieved from the first chinese ultraviolet - visible hyperspectral satellite instrument[J]. Engineering, 2024, 32: 106-115.
[83] YU Daihao, XIA Qiuwei, YU Saifen, et al. Elucidating CO_2 accumulation and dispersion in a semi-enclosed bay industrial park using Lidar and WRF-GHG modelling[J/OL]. EGU sphere[preprint], 2026. https://doi.org/10.5194/egusphere-2025-6470.
[84] YU Saifen, YU Daihao, XIA Qiuwei, et al. Spatiotemporal characteristics of atmospheric CO_2 under the influence of different industrial emission sources using lidar remote sensing in Nanping, China[J]. Journal of Environmental Sciences, 2026, 159: 490-501.
[85] HAN Haobin, WU Kenan, GUO Kexin, et al. All-fiber IPDA lidar for CH_4 leakage monitoring using InGaAs/InP single-photon detector[J]. Optics Express, 2024, 32(21): 37155-37166.
[86] GUO Kexin, HAN Haobin, LI Zhekai, et al. Simultaneous multi-gas detection using IPDA lidar with InGaAs/InP single-photon detector[J]. Optics and Laser Technology, 2026, 199: 115012.
[87] WANG Qin, FARHAN M, BU Lingbing, et al. Monitoring of atmospheric carbon dioxide over a desert site using

airborne and ground measurements[J]. Remote Sensing, 2022, 14(20): 5224.
[88] ZHANG Xuanye, ZHANG Miaomiao, BU Lingbing, et al. Simulation and error analysis of methane detection globally using spaceborne IPDA lidar[J]. Remote Sensing, 2023, 15(13): 3239.
[89] MAO Zhihua, ZHANG Yang, BU Lingbing, et al. Measurement of CO_2 column concentration above cloud tops with a spaceborne IPDA lidar[J]. Geophysical Research Letters, 2024, 51: e2024GL113309.
[90] LI Jiakun, XiongDUN, JIN Minglei, et al. Design of wide-band gas leak infrared imaging detection system[J]. Infrared and Laser Engineering, 2014, 43(6): 1966-1971.
李家琨, 顿雄, 金明磊, 等. 宽波段气体泄漏红外成像检测系统设计[J]. 红外与激光工程, 2014, 43(6): 1966-1971.
[91] YUAN Pan, TAN Zhuyan, ZHANG Xu, et al. Research on infrared imaging detection and differential spectrum filtering detection methods for industrial gas leakage[J]. Infrared and Laser Engineering, 2022, 51(8): 202107.
[92] Wang Minghe, SHENG Dian, YUAN Pan, et al. Infrared imaging detection for hazardous gas leakage using background information and improved YOLO networks[J]. Remote Sensing, 2025, 17(6): 1030.
[93] ARGALL P S, SICA R. Lidar: atmospheric sounding Introduction-sciencedirect[J]. Encyclopedia of Atmospheric Sciences (Second Edition), 2015, 262-269.
[94] MEI Liang, XU Ning, SONG Jiaming, et al. Research progress on temperature and humidity differential absorption lidar technology (invited)[J]. Acta Optica Sinica, 2025, 45(18): 1801002.
梅亮, 徐宁, 宋佳铭, 等. 温湿度差分吸收激光雷达技术研究进展(特邀)[J]. 光学学报, 2025, 45(18): 1801002.
[95] SAKAIZAWA D, NAGASAWA C, NAGAI T, et al. Development of a 1.6 μm differential absorption lidar with a quasi-phase-matching optical parametric oscillator and photon-counting detector for the vertical CO_2 profile[J]. Applied Optics, 2009, 48(4): 748-757.
[96] SPULER S M, REPASKY K S, MORLEY B, et al. Field-deployable diode-laser-based differential absorption lidar (DIAL) for profiling water vapor[J]. Atmospheric Measurement Techniques, 2015, 8(3): 1073-1087.
[97] WAGNER G A, PLUSQUELLIC D F. Multi-frequency differential absorption lidar system for remote sensing of CO_2 and H_2O near 1.6 μm[J]. Optics Express, 2018, 26(15): 19420-19434.
[98] MENG L, FIX A, WIRTH M, et al. Upconversion detector for range-resolved DIAL measurement of atmospheric CH_4[J]. Optics Express, 2018, 26(4): 3850-3860.
[99] YUE Bin, YU Saifen, DONG Jingjing, et al. Measurement methods and progress of greenhouse gas flux[J]. Acta Optica Sinica, 2023, 43(18): 259-271.
岳斌, 余赛芬, 董晶晶, 等. 温室气体通量测量方法及进展[J]. 光学学报, 2023, 43(18): 259-271.
[100] STROUD J R, WAGNER G A, PLUSQUELLIC D F. Multi-frequency differential absorption lidar (DIAL) system for aerosol and cloud retrievals of CO_2/H_2O and CH_4/H_2O[J]. Remote Sensing, 2023, 15(23): 5595.
[101] SHANGGUAN Mingjia, LIN Simin, GUO Xianghui, et al. High-range-resolution and long-distance CO_2 profiling using a single-photon differential absorption lidar[J]. Optics Letters, 2026, 51(1): 137-140.
[102] ZHU Tao, XUE Boyang, LI Hui, et al. Spatiotemporal detection of the carbon dioxide using a compact differential absorption lidar[J]. Microwave and Optical Technology Letters, 2025, 67: e70184.
[103] ABSHIRE J B, RAMANATHAN A, RIRIS H, et al. Airborne measurements of CO_2 column concentration and range using a pulsed direct-detection IPDA lidar[J]. Remote Sensing, 2014, 6(1): 443-469.
[104] HAN Ge, SHI Tianqi, MA Xin, et al. Obtaining gradients of XCO_2 in atmosphere using the constrained linear least-squares technique and multi-wavelength IPDA lidar[J]. Remote Sensing, 2020, 12(15): 2395.
[105] CHENG Chonghui, LIU Dong, WANG Shuaibo, et al. Estimating strong point CO_2 emissions by combining spaceborne IPDA lidar and HSRL[J]. Remote Sensing of Environment, 2025, 328: 114898.
[106] AI X, PEREZ-SERRANO A, QUATREVALET M, et al. Analysis of a random modulation single photon counting differential absorption lidar system for space-borne atmospheric CO_2 sensing[J]. Optics Express, 2016, 24(18): 21119-33.
[107] QUATREVALET M, AI X, PEREZ-SERRANO A, et al. Atmospheric CO_2 sensing with a random modulation continuous wave integrated path differential absorption lidar[J]. IEEE Journal of Selected Topics in Quantum Electronics, 2017, 23(2): 157-167.
[108] RIEKER G, GIORGETTA F, SWANN W, et al. Frequency-comb-based remote sensing of greenhouse gases over kilometer air paths[J]. Optica, 2014, 1(5): 290-298.
[109] HORIUCHI N. On-chip dual-comb source[J]. Nature Photonics, 2018, 4(3): e1701858.
[110] LOMSADZE B, CUNDIFF ST. Frequency combs enable rapid and high-resolution multidimensional coherent spectroscopy[J]. Science, 2017, 357(6358): 1389-1391.
[111] GIORGETTA F, PEISCHL J, HERMAN D, et al. Open-path dual-comb spectroscopy for multispecies trace gas detection in the 4.5-5 μm spectral region[J]. Laser & Photonics Reviews, 2021, 15(9): 2000583.
[112] HERMAN D, WEERASEKARA C, HUTCHERSOSN L, et al. Precise multispecies agricultural gas flux determined

using broadband open-path dual-comb spectroscopy[J]. Science Advances, 2021, 7(14): eabe9765.
[113] WESTBERG J, TENG C, CHEN Y, et al. Urban open-air chemical sensing using a mobile quantum cascade laser dual-comb spectrometer[J]. APL Photonics, 2023, 8: 120803.
[114] PATINO ROSAS W, CEZARD N. Greenhouse gas monitoring using an IPDA lidar based on a dual-comb spectrometer [J]. Optics Express, 2024, 32(8): 13614-13627.
[115] ZHONG Wei, LIU Yingyu, YIN Qin, et al. Broadband photon-counting dual-comb spectroscopy with attowatt sensitivity over turbulent optical paths[J]. Light: Science & Applications, 2025, 14: 293.
[116] ZHU Dongxu, WAN Zhuoren, MA Xiaoshuai, et al. Mode-programmable comb spectroscopy enabling non-cooperative computational sensing with single photon sensitivity[J/OL]. arXiv: 2511.16365, (2025). https://doi.org/10.48550/arXiv.2511.16365.
[117] RIRIS H, NUMATA K, LI S, et al. Airborne measurements of atmospheric methane column abundance using a pulsed integrated-path differential absorption lidar[J]. Applied Optics, 2012, 51(34): 8296-8305.
[118] ABSHIRE J, RIRIS H, WEAVER C, et al. Airborne measurements of CO_2 column absorption and range using a pulsed direct-detection integrated path differential absorption lidar[J]. Applied Optics, 2013, 52(19): 4446-4461.
[119] RIRIS H, RODRIGUEZ M, ALLAN G, et al. Pulsed airborne lidar measurements of atmospheric optical depth using the oxygen a-band at 765 nm[J]. Applied Optics, 2013, 52(25): 6369-6382.
[120] RIRIS H, RODRIGUEZ M, MAO J, et al. Airborne demonstration of atmospheric oxygen optical depth measurements with an integrated path differential absorption lidar[J]. Optics Express, 2017, 25(23): 29307-29327.
[121] WAGNER G, PLUSQUELLIC D. Ground-based, integrated path differential absorption lidar measurement of CO_2, CH_4, and H_2O near 1.6 μm[J]. Applied Optics, 2016, 55(23): 6292-6310.
[122] TITCHENER J, MILLINGTON-SMITH D, GOLDSACK C, et al. Single photon lidar gas imagers for practical and widespread continuous methane monitoring[J]. Applied Energy, 2022, 306: 118086.
[123] ZHU Shouzheng, LIU Shijie, TANG Guoliang, et al. Simulation evaluation of a single-photon laser methane remote sensor for leakage rate monitoring[J]. Optics Express, 2024, 32(7): 10962-10978.
[124] ZHU Shouzheng, LIU XU, ZHANG Yangyang, et al. Calibration and enhancement of an intensity-coded NIR laser single-photon system for quantitative methane leak monitoring[J]. Optics Express, 2026, 34: 1931-1945.
[125] SMITH R, CARDOSO A, MORLAND I, et al. Remote methane sensing using single-photon PPLN-waveguide upconversion lidar[J]. Optics Express, 2025, 33(13): 28177-28188.
[126] HAN Haobin, GUO Kexin, YI Li, et al. Remote sensing of flammable and toxic gases via IPDA lidar with InGaAs/InP single-photon detector over C+L band[J]. Optics Express, 2025, 33(18): 38828-38840.
[127] YU Saifen, ZHANG Zhen, XIA Haiyun. Simultaneous remote sensing of $HD^{16}O/H_2^{16}O$ profile using differential absorption lidar: a feasibility analysis[J]. Remote Sensing, 2026, 18(2): 221.
[128] YU Saifen, ZHANG Zhen, XIA Haiyun. Sensitivity analysis of simultaneous remote sensing of carbon dioxide and water vapor isotope using LiDAR[J]. Acta Optica Sinica, 2025, 45(6): 0601007.
余赛芬, 章振, 夏海云. 激光雷达同时遥感二氧化碳和水汽同位素的敏感性分析[J]. 光学学报, 2025, 45(6): 0601007.
[129] WALSH B, LEE H, BARNES N. Mid infrared lasers for remote sensing applications[J]. Journal of Luminescence, 2016, 169: 400-405.
[130] ZHENG Chuantao, HUANG Jianqiang, YE Weilin, et al. Demonstration of a portable near-infrared CH_4 detection sensor based on tunable diode laser absorption spectroscopy[J]. Infrared Physics & Technology, 2013, 61: 306-312.

Near-infrared Single-photon Lidar for Gas Remote Sensing: Technologies and Applications (Invited)

YI Li[1,2], HAN Haobin[1,2,3], LI Zhekai[1,2,3], XU Keyi[1,2], HU Jiadong[1,2,3], YU Saifen[1,2], ZHANG Zhen[1,2,3], XIA Haiyun[1,2,3]

(1 *School of Atmospheric Physics, Nanjing University of Information Science and Technology, Nanjing* 210044, *China*)

(2 *State Key Laboratory of Climate System Prediction and Risk Management, NUIST, Nanjing* 210044, *China*)

(3 *Institute of Lidar Technology, GuangZai Co. Ltd., Hangzhou* 310005, *China*)

Abstract: The near-infrared spectral range serves as a distinctive absorption region for various greenhouse and pollutant gases, offering advantages such as high atmospheric transmittance and low background noise.

Despite these benefits, traditional detectors are limited in their sensitivity within this wavelength range. The integration of single-photon detection technology presents a promising solution to overcome the challenges associated with detecting weak echo signals, thereby enhancing system detection range and precision. Current technologies and applications of near-infrared single-photon lidar for gas remote sensing are classified and compared.

This review focuses on the relationship between detector characteristics, lidar detection mechanisms, and practical gas sensing performance, with emphasis on the applicability of different technical routes under atmospheric and industrial monitoring conditions. This review compares the main types of near-infrared single-photon detectors, including photomultiplier tubes, single-photon avalanche diodes, superconducting nanowire single-photon detectors, and upconversion single-photon detectors. The comparison is conducted in terms of key performance metrics, including quantum efficiency, dark count rate, timing resolution, and system integration complexity, since these parameters directly influence lidar sensitivity and retrieval accuracy under weak-return conditions. We evaluate these metrics to determine each detector′s advantages and suitable applications in gas remote sensing. The review also divides existing gas remote sensing lidar systems into three types based on their detection mechanisms: differential absorption lidar, integrated path absorption lidar, and differential absorption spectroscopy lidar. The classification is further refined according to implementation details, with integrated path absorption lidar being subdivided into integrated path differential absorption, integrated path dual-comb spectroscopy, and integrated path scanning absorption spectroscopy. The review framework therefore combines detector-level comparison with retrieval-principle classification, enabling a structured assessment of near-infrared single-photon gas sensing systems reported in the literature.

Photomultiplier tubes exhibit mature photon-counting capability and stable timing performance in visible wavelengths, but their direct response in the near-infrared spectral region remains limited. InGaAs/InP single-photon avalanche diodes are ideal for room-temperature fiber-integrated systems because of their compact structure, relatively low operating requirements, and compatibility with communication-band optical components, although their performance is affected by dark counts and afterpulse effects under high count-rate operation. Superconducting nanowire single-photon detectors provide optimal detection efficiency under cryogenic conditions and demonstrate advantages including extremely low dark count rates, high timing precision, and broad spectral response, making them suitable for long-range and ultra-weak signal detection. Upconversion single-photon detectors enable low-noise visible-light detection of near-infrared signals through frequency upconversion. By converting near-infrared photons into visible wavelengths through nonlinear optical processes, upconversion single-photon detectors combine the low-noise characteristics of visible single-photon detectors with the spectral advantages of near-infrared lidar systems. Their performance is closely related to pump laser stability, conversion efficiency, and optical coupling conditions. In addition to detector efficiency, practical lidar performance is also influenced by dead time, maximum photon-counting rate, optical alignment stability, and thermal control conditions. Therefore, the applicability of different detector technologies depends not only on laboratory detection capability but also on overall system integration requirements and measurement scenarios. With these detector characteristics as the basis, the lidar architectures themselves can then be compared in terms of how effectively they translate single-photon sensitivity into measurable gas information. Differential absorption lidar uses atmospheric backscatter echoes to obtain gas concentration profiles, making it suitable for concentration profiling. Integrated path absorption lidar measures concentration through reflection from hard targets, making it suitable for satellite, airborne, and leakage monitoring on the ground. Differential absorption spectroscopy lidar combines distance and spectral resolution, representing an advanced approach for multi-component, high-precision remote sensing. Representative systems, performance metrics, and applicable scenarios for each lidar technology are analyzed in detail. This review indicates that the adoption of single-photon detection not only improves sensitivity but also reduces transmitter power requirements and promotes the development of compact and portable lidar systems. In addition, the literature shows that single-photon differential absorption lidar has been used for range-resolved profiling of CO_2, CH_4, and H_2O under weak-backscatter conditions; integrated path differential absorption has supported column measurements and is less sensitive to footprint mismatch in moving-platform observations; integrated path dual-comb spectroscopy has extended photon-counting remote sensing to broadband path-integrated spectroscopy over kilometer-scale paths; and integrated path scanning absorption spectroscopy has shown

particular value in leakage monitoring and multi-gas discrimination under strong background-light conditions. Differential absorption spectroscopy lidar further demonstrates the feasibility of simultaneous range-resolved and spectrally resolved retrievals, including cases involving overlapping absorption features such as CO_2 and HDO. However, several limitations remain evident across existing systems, including detector noise accumulation, limited dynamic range, spectral interference in multi-component detection, and the requirement for long signal integration times under ultra-weak signal conditions.

In conclusion, near-infrared single-photon detection technology has significantly advanced gas remote sensing towards higher sensitivity, multi-component detection, and miniaturization. However, challenges remain, including dark counts and afterpulse suppression in room-temperature detectors, crosstalk and data fusion in multi-gas simultaneous detection, and system stability for long-term field deployment. Future research should focus on extending into the mid-infrared range to exploit stronger molecular absorption lines, developing high-photon-counting-rate detectors to improve dynamic range, and advancing integrated photonics architectures for compact, low-power, field-deployable multi-gas monitoring systems.

Key words: Single-photon detection; Infrared gas remote sensing; Differential absorption; Path-integrated; Spectral remote sensing

OCIS Codes: 280.1910; 280.3640; 030.5260; 280.4788; 300.6340

CSTR: 32255.14.gzxb20265505.0555210

Foundation item: National Natural Science Foundation of China (42405138, 42305147)